BMC
Neurology

**RESEARCH ARTICLE**                                    **Open Access**

# Subregional 6-[$^{18}$F]fluoro-L-$m$-tyrosine Uptake in the Striatum in Parkinson's Disease

Sayaka Asari[1*], Ken-ichi Fujimoto[1], Akihiro Miyauchi[2], Toshihiko Sato[3], Imaharu Nakano[1] and Shin-ichi Muramatsu[1*]

## Abstract

**Background:** In idiopathic Parkinson's disease (PD) the clinical features are heterogeneous and include different predominant symptoms. The aim of the present study was to determine the relationship between subregional aromatic l-amino acid decarboxylase (AADC) activity in the striatum and the cardinal motor symptoms of PD using high-resolution positron emission tomography (PET) with an AADC tracer, 6-[$^{18}$F]fluoro-L-$m$-tyrosine (FMT).

**Methods:** We assessed 101 patients with PD and 19 healthy volunteers. PD was diagnosed based on the UK Brain Bank criteria by two experts on movement disorders. Motor symptoms were measured with the Unified Parkinson's Disease Rating Scale (UPDRS). FMT uptake in the subregions of the striatum was analyzed using semi-automated software for region-of-interest demarcation on co-registered magnetic resonance images.

**Results:** In all PD patients, FMT uptake was decreased in the posterior putamen regardless of predominant motor symptoms and disease duration. Smaller uptake values were found in the putamen contralateral to the side with more affected limbs. The severity of bradykinesia, rigidity, and axial symptoms was correlated with the decrease of FMT uptake in the putamen, particularly in the anterior part. No significant correlation was observed between tremors and FMT uptake.

**Conclusions:** Decrease of FMT uptake in the posterior putamen appears to be most sensitive in mild PD and uptake in the anterior putamen may reflect the severity of main motor symptoms, except for tremor.

## Background

Cardinal motor symptoms such as bradykinesia, rigidity, and tremor in Parkinson's Disease (PD) become apparent after a depletion of dopamine in the striatum to approximately 20% of normal levels and a reduction in aromatic L-amino acid decarboxylase (AADC) activity to 5%-20% of normal levels [1,2]. In PD, dopaminergic hypofunction in the striatum is not homogenous in association with the selective loss of ventral intermediate and lateral cell groups of the substantia nigra pars compacta that project to the posterior part of the striatum [3], although the reason for this selective vulnerability remains unknown.

Positron emission tomography (PET) is valuable for assessing altered dopamine function in PD. The first tracer used to visualize and assess the integrity of dopamine presynaptic systems was 6-[$^{18}$F]fluoro-L-dopa (FDOPA), a fluoro-analog of L-dopa [4]. FDOPA is taken up into the dopaminergic axon terminals and decarboxylated by AADC before being trapped and stored in synaptic vesicles. FDOPA uptake is highly correlated with viable dopaminergic cells in neurotoxin-lesioned monkeys [5] and in postmortem human PD brains [6]. A shortcoming complicating the use of this agent, however, is that metabolites of FDOPA (such as 3-$O$-methyl-[$^{18}$F]fluoro-L-dopa, which is formed by the action of the ubiquitous enzyme catechol-$O$-methyl-transferase (COMT)) enter the brain and diminish image contrast. An alternative agent is the non-catecholic tracer 6-[$^{18}$F] fluoro -L-$m$-tyrosine (FMT). FMT is also a good substrate for AADC but is not metabolized by COMT; thus, FMT uptake has approximately twice the sensitivity of FDOPA uptake and more fully represents the extent of AADC activity [7-10].

To elucidate the relationship between the main motor symptoms of PD and subregional AADC activity in the striatum, we applied a semi-automated segmentation method for extracting putaminal subregions from

* Correspondence: sasari@jichi.ac.jp; muramats@jichi.ac.jp
[1]Division of Neurology, Department of Medicine, Jichi Medical University, Tochigi, Japan
Full list of author information is available at the end of the article

high-resolution FMT PET images that were co-registered with 3.0-tesla magnetic resonance (MR) images.

## Methods

### Subjects and clinical evaluation

Our sample consisted of 101 patients with PD and 19 healthy individuals. PD was diagnosed clinically according to the UK PD Society Brain Bank criteria [11]. All of the patients had bradykinesia and at least one of the three features of PD: 4-6 Hz resting tremor, rigidity, and postural instability. All of the patients had asymmetric onset and showed a positive response to dopaminergic medication. None exhibited atypical symptoms such as severe gaze palsy or symptomatic dysautonomia. The control group included healthy individuals with no history of neurologic or psychiatric diseases.

Motor symptoms were evaluated using the motor examination part of the Unified Parkinson's Disease Rating Scale (UPDRS). Motor subscores were determined as follows: tremor (motor UPDRS: 20 + 21), bradykinesia (motor UPDRS: 23 + 24 + 25 + 26), rigidity (motor UPDRS: 22), and axial (motor UPDRS: 18 + 19 + 27 + 28 + 29 + 30 + 31). The mini-mental state examination (MMSE) was used to assess cognitive function.

This study was approved by the Institutional Ethics Committee of Jichi Medical University and all participants gave written informed consent.

### PET imaging

All patients stopped levodopa at least 16 h before PET. To increase the availability of the tracer, all subjects took 2.5 mg/kg of carbidopa (a peripheral AADC inhibitor) orally 1 h before FMT injection. Prior to the emission scan, a 10 min transmission scan was obtained for attenuation correction. Subsequently, 0.12 mCi/kg of FMT in saline was infused into an antecubital vein and a 30-90 min static three-dimensional acquisition was started simultaneously using a PET-CT (GEMINI GXL, Philips, Amsterdam, The Netherlands). Each subject also underwent 3.0-tesla MR imaging (Achieva 3.0 T, Philips) using an inversion recovery (IR) proton density (PD)-weighted pulse sequence to enhance the contrast of anatomical structures. The PET and MR imaging data were co-registered with a fusion processing program (Syntegra, Philips) to produce fusion images. This program provided manual and point-based image registration as well as automated methods of gray-value-based image registration, including a mutual information algorithm [12]. In addition, an adaptive level set of segmentation was used for coregistration of CT and MRI imaging data [13].

### Semi-automated region of interest analysis

Regions-of-interest (ROIs) in the putamen and caudate nucleus were defined in three dimensions (3-D)

bilaterally on the co-registered MR images where the striatum was best visualized. The putamen and the head of caudate nucleus were delineated by manual inspection on the three to five adjacent MR planes that corresponded to those planes on the PET images. The putamen was then automatically divided into three parts in the rostrocaudal direction using dedicated software for ROI demarcation. The 3-D ROIs (volumes of interest, VOIs) were extracted automatically by connecting two-dimensional drawings on each plane using a linear interpolation algorithm for VOI outlines. For reference, cerebellar ROIs were also defined in 3-D and located bilaterally on the cerebellar cortex.

Striatal-to-cerebellum ratio (SCR) values of radioactivity counts were calculated in the 80-90-min frame for each structure, using bilaterally averaged cerebellar ROI data as the denominator. For subregional analysis of their association with major motor symptoms in the PD subjects, SCR values from the caudate nucleus and each part of the putamen were analyzed on the contralateral to the more affected side of limb.

### Statistical Analysis

For comparison of more than two groups, one-way analysis of variance (ANOVA) was used. When the one-way ANOVA was significant at $p < 0.05$, post-hoc comparisons were conducted using Scheffé's test. We examined the correlation of FMT uptake in each part of the putamen with disease duration, and with the symptoms of bradykinesia, tremor, rigidity, and postural instability assessed on UPDRS motor scores. Non-linear exponential regression analysis was applied to assess the relationship between FMT uptake and disease duration (Prism, GraphPad Software, La Jolla, CA). SCR values and the UPDRS scores were compared by Spearman's rank correlation coefficient test. $P < 0.05$ was considered to indicate a statistically significant difference.

## Results

### Characteristics of subjects

Demographic and clinical characteristics of the patients with PD and those of the control subjects are listed in Table 1 and Table 2. The mean ages of the PD patients (41 male and 60 female) and the control subjects (6 male and 13 female) were 64.0 years (SD 9.3) and 56.7

**Table 1 Clinical Characteristics of the Subjects**

| Characteristics | PD | Normal Control | p value |
|---|---|---|---|
| Age, year, mean ± SD | 64.0 ± 9.3 | 56.7 ± 11.1 | 0.005 |
| Male/Female | 41/60 | 6/13 | 0.542 |
| MMSE | 27 ± 2.6 | 29 ± 1.3 | 0.005 |

MMSE, Mini Mental State Examination.
Data are given as mean ± standard deviation (SD) values.

**Table 2 Clinical Charasteristics of the PD patients**

| | |
|---|---|
| Symptom duration, year | 6.0 ± 4.4 |
| More affected side | Right 55/Left 46 |
| Hoehn-Yahr stage, on | 2.4 ± 0.9 |
| Hoehn-Yahr stage, off | 3.3 ± 1.1 |
| UPDRS score | |
| Total motor | 30.3 ± 16 |
| Bradykinesia | 9.86 ± 6.3 |
| Rigidity | 6.15 ± 3.8 |
| Axial | 9.54 ± 6.2 |
| Tremor | 4.80 ± 4.0 |

UPDRS, Unified Parkinson's Disease Rating Scale.

Data are given as mean ± standard deviation (SD) values.

years (SD 11.1), respectively. A wide range of duration and severity of symptoms was represented among the patients. The mean duration of symptoms was 6.0 years (SD 4.4) and the mean UPDRS motor score was 30.3 (SD 16.0). The right side was more affected in 55 patients.

## Subregional analysis of FMT uptake

Figure 1 shows representative images of FMT uptake in a normal subject and in early- and late-stage PD patients. Among the patients, FMT uptake showed the most marked decrease in the posterior putamen, regardless of disease duration, but significant decrease was seen throughout the striatum compared with the healthy controls. There were significant differences between side (ipsi- vs. contralateral to the more affected limbs), region (anterior vs. posterior putamen), and diagnosis (healthy subjects vs. PD group) ($P < 0.001$) (Figure 2a). Asymmetry between the striatum of the more and less
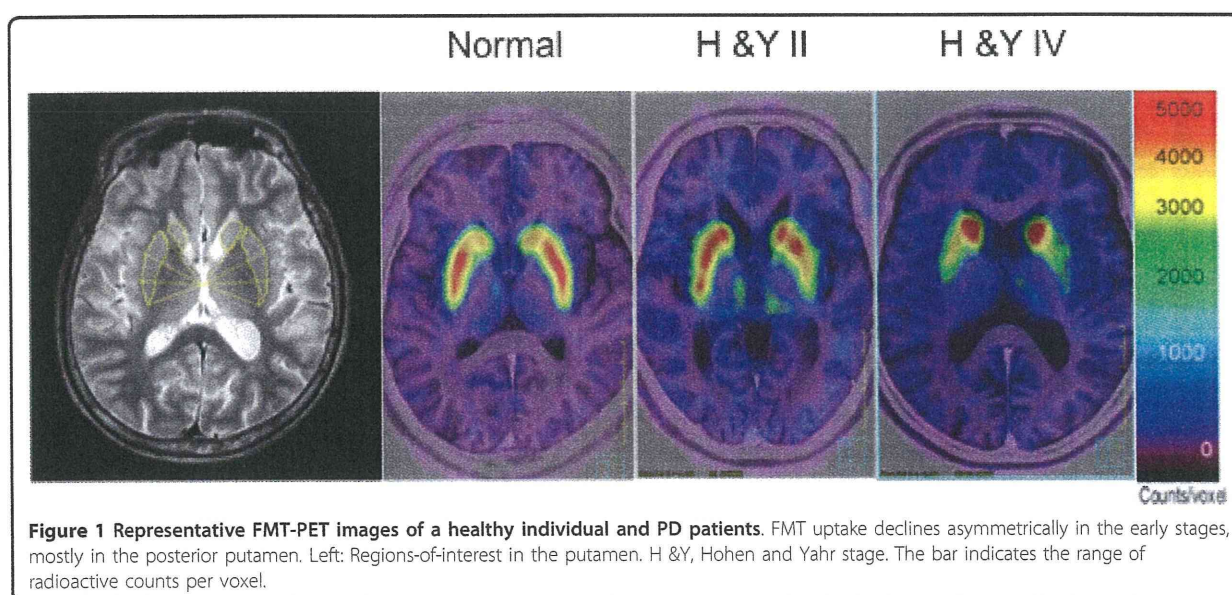
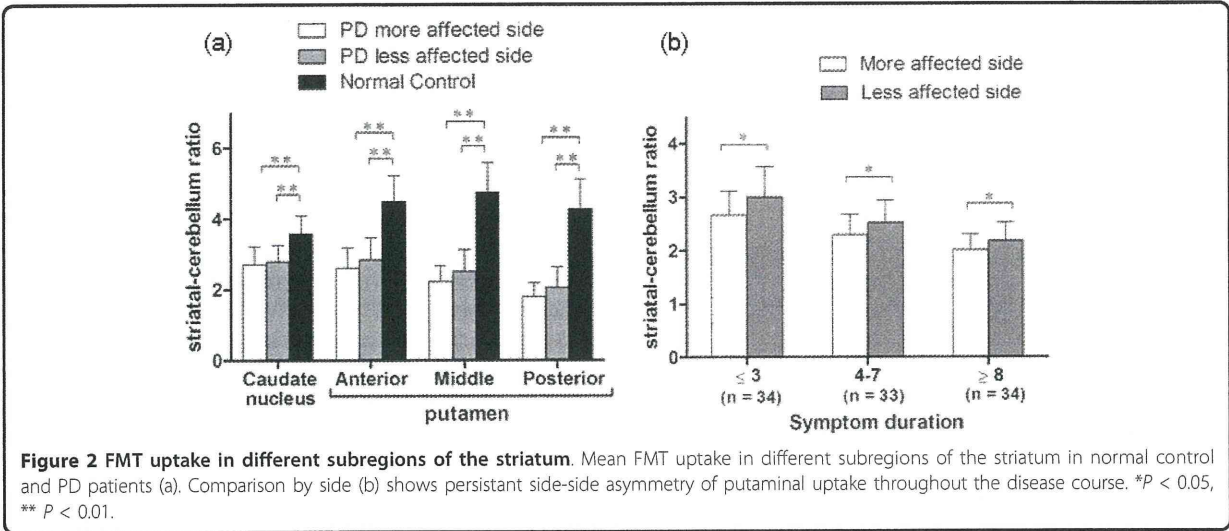affected sides is preserved, but shows a decrease with disease progression (Figure 2b).

## Decline in FMT uptake with disease duration

Figure 3 shows scatterplots of FMT uptake against symptom duration in three regions of the putamen contralateral to the more affected limbs. Because age-related factors such as age at onset of symptoms and age-related Alzheimer-type pathology may influence disease duration, we excluded elderly-onset patients (> 70 years old; $n = 19$) in this analysis. Exponential regression curves that best fitted the data for each of the three regions analyzed are superimposed on the figure. Between 10 and 15 years of symptom duration, the FMT for all three curves leveled off to constant values that showed a statistically significant difference between the anterior and posterior putamen ($p < 0.001$). In the control group, there was no significant difference in SCR of FMT uptake between younger (< 59 years old, $n = 10$) and older (≥ 60 years old, $n = 9$) subjects (putamen, $p = 0.87$; caudate, $p = 0.81$).
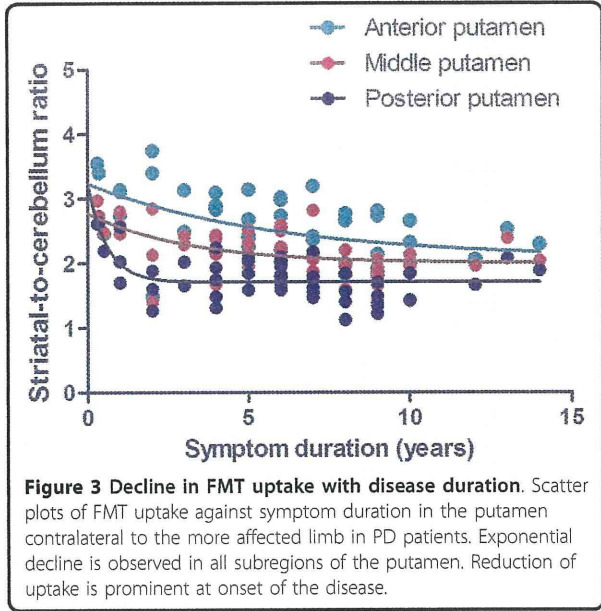
## Correlation of cardinal symptoms and FMT uptake

To minimize the possibility of including patients with alternative diagnoses, we analyzed patients who had cardinal motor symptoms for at least 3 years ($n = 42$). We obtained positive correlations between the severities of major motor symptoms: rigidity vs. axial symptoms ($r = 0.68$, $p < 0.001$), rigidity vs. bradykinesia ($r = 0.56$, $p < 0.001$), bradykinesia vs. postural instability ($r = 0.54$, $p < 0.001$), and tremor vs. bradykinesia ($r = 0.39$, $p = 0.014$). However, tremor did not have a significant relation with rigidity ($r = 0.20$, $p = 0.20$) or with axial symptoms ($r = $



**Figure 1 Representative FMT-PET images of a healthy individual and PD patients.** FMT uptake declines asymmetrically in the early stages, mostly in the posterior putamen. Left: Regions-of-interest in the putamen. H &Y, Hohen and Yahr stage. The bar indicates the range of radioactive counts per voxel.

**Figure 2 FMT uptake in different subregions of the striatum**. Mean FMT uptake in different subregions of the striatum in normal control and PD patients (a). Comparison by side (b) shows persistant side-side asymmetry of putaminal uptake throughout the disease course. *$P < 0.05$, ** $P < 0.01$.

0.12, $p = 0.45$). Axial symptoms, rigidity, and bradykinesia scores showed a correlation with FMT uptake in the contralateral putamen, with the highest correlation in the anterior putamen, but not in the contralateral caudate (Table 3). No significant correlation was evident between unilateral tremor scores from the most severely affected limbs and any of the striatal regions. To assess the potential influence of age, we analyzed older patients (> 60 years old; $n = 25$) separately and found similar correlations between major symptoms and FMT uptake (Table 4).



**Figure 3 Decline in FMT uptake with disease duration**. Scatter plots of FMT uptake against symptom duration in the putamen contralateral to the more affected limb in PD patients. Exponential decline is observed in all subregions of the putamen. Reduction of uptake is prominent at onset of the disease.

## Discussion

Idiopathic PD is defined as a synucleinopathy in which Lewy bodies, pathological aggregations of the synaptic protein α-synuclein, are found in the dopaminergic neurons in the substantia nigra [14,15]. A reduction of dopamine in the striatum is a consistent finding in PD, although the clinical features are heterogeneous and include different predominant symptoms (resting tremor, bradykinesia, rigidity, or postural instability and gait disorder) with different rates of progression, and with or without dementia [16-19]. PET imaging is a valuable tool for assessing altered dopaminergic function in the striatum in PD. While FDOPA is suitable for assessing the metabolism of levodopa, FMT is superior for estimating AADC activity because it enables the production of higher-quality brain images [7,20-22]. The high resolution of FMT-PET images enables analysis of

**Table 3 Correlations of UPDRS scores and FMT uptake ratio values in the each part of the putamen**

| Putamen | Anterior | Middle | Posterior | Whole |
|---|---|---|---|---|
| Symptom duration, year | -0.52 (<0.001) | -0.56 (<0.001) | -0.51 (<0.001) | -0.58 (<0.001) |
| Total motor score | -0.56 (<0.001) | -0.48 (0.002) | -0.41 (0.008) | -0.51 (0.001) |
| Bradykinesia | -0.54 (<0.001) | -0.53 (<0.001) | -0.44 (0.005) | -0.55 (<0.001) |
| Rigidity | -0.50 (0.001) | -0.43 (0.006) | -0.37 (0.018) | -0.44 (0.005) |
| Axial | -0.60 (<0.001) | -0.51 (0.001) | -0.37 (0.016) | -0.50 (0.001) |
| Tremor | 0.069 (0.658) | 0.085 (0.587) | 0.015 (0.925) | 0.050 (0.747) |

Data are given as $r$ ($p$) values. These values were calculated by Spearman's rank correlation coefficient test. UPDRS motor score in off-medication state was evaluated in 42 subjects.

**Table 4 Correlations of UPDRS scores and FMT uptake ratio values in the each part of the putamen in elder patients**

| Putamen | Anterior | Middle | Posterior | Whole |
|---|---|---|---|---|
| Symptom duration, year | -0.70 (<0.001) | -0.63 (<0.005) | -0.45 (<0.05) | -0.70 (<0.001) |
| Total motor score | -0.56 (<0.01) | -0.50 (<0.05) | -0.37 (0.07) | -0.49 (<0.05) |
| Bradykinesia | -0.46 (<0.05) | -0.46 (<0.05) | -0.34(0.08) | -0.46 (<0.05) |
| Rigidity | -0.46 (<0.05) | -0.39 (0.05) | -0.31 (0.12) | -0.37 (0.06) |
| Axial | -0.69 (<0.001) | -0.59 (<0.01) | -0.45 (<0.05) | -0.58 (<0.01) |
| Tremor | 0.26 (0.21) | 0.12 (0.58) | 0.06 (0.77) | 0.14 (0.51) |

Data are given as $r$ ($p$) values. These values were calculated by Spearman's rank correlation coefficient test. UPDRS motor score in off-medication state was evaluated in 25 subjects.

dopaminergic presynaptic changes in each subregion of the striatum.

In the present study, FMT uptake in PD was reduced in the putamen, particularly in the posterior part. The anterior-to-posterior gradient of the uptake decrease in the putamen persisted to the advanced stage of PD. These results are consistent with those of previous reports that used other tracers of presynaptic dopaminergic terminals, and are considered to reflect the selective degeneration of nigrostriatal pathways that project into the posterior part of the putamen [23-25]. The lowest value of FMT uptake was observed in the posterior part of the putamen contralateral to the more affected limbs, even in the early stage of the disease. Because we analyzed regions in the posterior one-third of the putamen on high-resolution images, it is unlikely that the decreases in uptake were caused by partial volume effects, which may arise from placement of a small ROI on inaccurately co-registered images.

Post-mortem investigations of PD demonstrate that the rate of decrease of nigral neurons is rapid in the initial stage of the disease: approximately 40%-50% are lost in the first decade, possibly with a slower rate of degeneration later on, to finally approach a normal age-related linear decline [26]. In the present study, loss of FMT was well fitted to symptom duration using a single exponential approximation. The exponential model provided a better fit than a linear model, indicating that the rate of decline in FMT uptake in the contralateral putamen was faster at the beginning of the disease and slowed down as the disease progressed, in agreement with the results of previous studies that used radiotracers for imaging nigrostriatal nerve terminals [23-25]. Because we performed cross-sectional analysis in the present study, and because all of the participants were on medication, the data do not provide accurate information

regarding the natural course of the disease, even if PET measurements were taken in off-medication state. Even so, the present data are important for assessing the progression of dopaminergic hypofunction in the striatum under optimal medical treatment, and can provide the basis for the development of even better therapeutic strategies [27,28].

We applied striatal count ratios to analyze the relationships between subregional putaminal FMT uptake and clinical symptoms. Striatal count ratios using the cerebellum as the denominator have a strong correlation with striatal uptake constants (Ki values) [29,30]. The present FMT-PET study showed a significant correlation between cardinal motor symptoms (rigidity, bradykinesia, and axial symptoms) and uptake of the tracer in the putamen, and no significant correlation was found between tremor score and FMT uptake. These findings are consistent with the results of previous PET studies [31-33]. The clinical correlations were more significant in the anterior part of the putamen than in the posterior part, possibly reflecting a floor effect for the uptake of FMT in the posterior part of the putamen, where the decrease was severe even in the early stage of the disease.

The pathophysiological mechanism of tremor is not fully understood [34]. Tremor does not respond to L-dopa as well as do bradykinesia and rigidity. The fact that stereotactic lesion or deep brain stimulation of the ventral intermediate nucleus (Vim) of the thalamus successfully improves tremor indicates a strong association between non-dopaminergic thalamic and cerebellar systems, and tremor generation [35,36].

## Conclusions

Our results indicate that FMT-PET is useful for evaluating PD patients from the early stage of the disease and for studying the relationship between AADC activity and various clinical features. Decrease of FMT uptake in the posterior putamen appears to be most sensitive in mild PD, and uptake in the anterior putamen may reflect the severity of main motor symptoms, except for tremor. These data provide an important baseline for evaluating the effects of surgical interventions, such as gene therapy for PD.

**Author details**
[1]Division of Neurology, Department of Medicine, Jichi Medical University, Tochigi, Japan. [2]WebNet Technology, Tochigi, Japan. [3]Utsunomiya Central Clinic, Tochigi, Japan.

## Authors' contributions

SA participated in designing the study, data collection, conducted the statistical analyses, interpreted data and drafted the first manuscript. KF participated in data collection and interpretation of data. AM participated in data collection and interpretation of data. TS participated in data collection and interpretation of data. IN participated in designing the study and interpretation of data. SM conceived the study, participated in its design, data collection, interpretation of data and drafting the manuscript. All authors read and approved the final manuscript.

## Competing interests

The authors declare that they have no competing interests.

## References

1. Hornykiewicz O: Biochemical aspects of Parkinson's disease. *Neurology* 1998, 51:S2-9.
2. Nagatsu T, Ichinose H: Molecular biology of catecholamine-related enzymes in relation to Parkinson's disease. *Cell Mol Neurobiol* 1999, 19:57-66.
3. Halliday G: Substantia nigra and locus coeruleus. In *The human nervous system*. 2 edition. Edited by: Paxinos G, Mai JK. Amsterdam; Boston: Elsevier Academic Press; 2004:pp457-458.
4. Garnett ES, Firnau G, Nahmias C: Dopamine visualized in the basal ganglia of living man. *Nature* 1983, 305:137-138.
5. Pate BD, Kawamata T, Yamada T, McGeer EG, Hewitt KA, Snow BJ, Ruth TJ, Calne DB: Correlation of striatal fluorodopa uptake in the MPTP monkey with dopaminergic indices. *Ann Neurol* 1993, 34:331-338.
6. Snow BJ, Tooyama I, McGeer EG, Yamada T, Calne DB, Takahashi H, Kimura H: Human positron emission tomographic [$^{18}$F]fluorodopa studies correlate with dopamine cell counts and levels. *Ann Neurol* 1993, 34:324-330.
7. DeJesus OT, Flores LG, Murali D, Converse AK, Bartlett RM, Barnhart TE, Oakes TR, Nickles RJ: Aromatic l-amino acid decarboxylase turnover in vivo in rhesus macaque striatum: a microPET study. *Brain Res* 2005, 1054:55-60.
8. DeJesus OT, Holden JE, Endres C, Murali D, Oakes TR, Shelton S, Uno H, Houser D, Freund L, Perlman SB, et al: Visualization of dopamine nerve terminals by positron tomography using [$^{18}$F]fluoro-β-fluoromethylene-m-tyrosine. *Brain Res* 1992, 597:151-154.
9. Doudet DJ, Chan GL, Jivan S, DeJesus OT, McGeer EG, English C, Ruth TJ, Holden JE: Evaluation of dopaminergic presynaptic integrity: 6-[$^{18}$F] fluoro-l-dopa versus 6-[$^{18}$F]fluoro-l-m-tyrosine. *J Cereb Blood Flow Metab* 1999, 19:278-287.
10. Eberling JL, Bankiewicz KS, O'Neil JP, Jagust WJ: PET 6-[$^{18}$F]fluoro-l-m-tyrosine Studies of Dopaminergic Function in Human and Nonhuman Primates. *Front Hum Neurosci* 2007, 1:9.
11. Hughes AJ, Daniel SE, Lees AJ: Improved accuracy of clinical diagnosis of Lewy body Parkinson's disease. *Neurology* 2001, 57:1497-1499.
12. Maes F, Collignon A, Vandermeulen D, Marchal G, Suetens P: Multimodality image registration by maximization of mutual information. *IEEE Trans Med Imaging* 1997, 16:187-198.
13. Wells WM, Grimson WL, Kikinis R, Jolesz FA: Adaptive segmentation of MRI data. *IEEE Trans Med Imaging* 1996, 15:429-442.
14. Dickson DW, Braak H, Duda JE, Duyckaerts C, Gasser T, Halliday GM, Hardy J, Leverenz JB, Del Tredici K, Wszolek ZK, Litvan I: Neuropathological assessment of Parkinson's disease: refining the diagnostic criteria. *Lancet Neurol* 2009, 8:1150-1157.
15. Spillantini MG, Schmidt ML, Lee VM, Trojanowski JQ, Jakes R, Goedert M: Alpha-synuclein in Lewy bodies. *Nature* 1997, 388:839-840.
16. Halliday GM, McCann H: The progression of pathology in Parkinson's disease. *Ann N Y Acad Sci* 2010, 1184:188-195.
17. Maetzler W, Liepelt I, Berg D: Progression of Parkinson's disease in the clinical phase: potential markers. *Lancet Neurol* 2009, 8:1158-1171.
18. Selikhova M, Williams DR, Kempster PA, Holton JL, Revesz T, Lees AJ: A clinico-pathological study of subtypes in Parkinson's disease. *Brain* 2009, 132:2947-2957.
19. van Rooden SM, Heiser WJ, Kok JN, Verbaan D, van Hilten JJ, Marinus J: The identification of Parkinson's disease subtypes using cluster analysis: a systematic review. *Mov Disord* 2010, 25:969-978.
20. Brown WD, DeJesus OT, Pyzalski RW, Malischke L, Roberts AD, Shelton SE, Uno H, Houser WD, Nickles RJ, Holden JE: Localization of trapping of 6-[$^{18}$F]fluoro-l-m-tyrosine, an aromatic l-amino acid decarboxylase tracer for PET. *Synapse* 1999, 34:111-123.
21. DeJesus OT, Haaparanta M, Solin O, Nickles RJ: 6-fluoroDOPA metabolism in rat striatum: time course of extracellular metabolites. *Brain Res* 2000, 877:31-36.
22. Elsinga PH, Hatano K, Ishiwata K: PET tracers for imaging of the dopaminergic system. *Curr Med Chem* 2006, 13:2139-2153.
23. Bruck A, Aalto S, Rauhala E, Bergman J, Marttila R, Rinne JO: A follow-up study on 6-[$^{18}$F]fluoro-l-dopa uptake in early Parkinson's disease shows nonlinear progression in the putamen. *Mov Disord* 2009, 24:1009-1015.
24. Lee CS, Schulzer M, de la Fuente-Fernandez R, Mak E, Kuramoto L, Sossi V, Ruth TJ, Calne DB, Stoessl AJ: Lack of regional selectivity during the progression of Parkinson disease: implications for pathogenesis. *Arch Neurol* 2004, 61:1920-1925.
25. Nandhagopal R, Kuramoto L, Schulzer M, Mak E, Cragg J, Lee CS, McKenzie J, McCormick S, Samii A, Troiano A, et al: Longitudinal progression of sporadic Parkinson's disease: a multi-tracer positron emission tomography study. *Brain* 2009, 132:2970-2979.
26. Fearnley JM, Lees AJ: Ageing and Parkinson's disease: substantia nigra regional selectivity. *Brain* 1991, 114(Pt 5):2283-2301.
27. Christine CW, Starr PA, Larson PS, Eberling JL, Jagust WJ, Hawkins RA, VanBrocklin HF, Wright JF, Bankiewicz KS, Aminoff MJ: Safety and tolerability of putaminal AADC gene therapy for Parkinson disease. *Neurology* 2009, 73:1662-1669.
28. Muramatsu S, Fujimoto KI, Kato S, Mizukami H, Asari S, Ikeguchi K, Kawakami T, Urabe M, Kume A, Sato T, et al: A Phase I study of aromatic l-amino acid decarboxylase gene therapy for Parkinson's disease. *Mol Ther* 2010, 18:1731-1735.
29. Dhawan V, Ma Y, Pillai V, Spetsieris P, Chaly T, Belakhlef A, Margouleff C, Eidelberg D: Comparative analysis of striatal FDOPA uptake in Parkinson's disease: ratio method versus graphical approach. *J Nucl Med* 2002, 43:1324-1330.
30. Eberling JL, Pivirotto P, Bringas J, Bankiewicz KS: Comparison of two methods for the analysis of [$^{18}$F]6-fluoro-l-m-tyrosine PET data. *Neuroimage* 2004, 23:358-363.
31. Martin WR, Wieler M, Stoessl AJ, Schulzer M: Dihydrotetrabenazine positron emission tomography imaging in early, untreated Parkinson's disease. *Ann Neurol* 2008, 63:388-394.
32. Otsuka M, Ichiya Y, Kuwabara Y, Hosokawa S, Sasaki M, Yoshida T, Fukumura T, Masuda K, Kato M: Differences in the reduced $^{18}$F-Dopa uptakes of the caudate and the putamen in Parkinson's disease: correlations with the three main symptoms. *J Neurol Sci* 1996, 136:169-173.
33. Vingerhoets FJ, Schulzer M, Calne DB, Snow BJ: Which clinical sign of Parkinson's disease best reflects the nigrostriatal lesion? *Ann Neurol* 1997, 41:58-64.
34. Rodriguez-Oroz MC, Jahanshahi M, Krack P, Litvan I, Macias R, Bezard E, Obeso JA: Initial clinical manifestations of Parkinson's disease: features and pathophysiological mechanisms. *Lancet Neurol* 2009, 8:1128-1139.
35. Diamond A, Shahed J, Jankovic J: The effects of subthalamic nucleus deep brain stimulation on parkinsonian tremor. *J Neurol Sci* 2007, 260:199-203.
36. Terao T, Yokochi F, Taniguchi M, Kawasaki T, Okiyama R, Hamada I, Nishikawa N, Izawa N, Shin M, Kumada S, Takahashi H: Microelectrode findings and topographic reorganisation of kinaesthetic cells after gamma knife thalamotomy. *Acta Neurochir (Wien)* 2008, 150:823-827, discussion 827.

Brief Communication

# Preclinical substantia nigra dysfunction in rapid eye movement sleep behaviour disorder

Masayuki Miyamoto [a,*], Tomoyuki Miyamoto [a], Masaoki Iwanami [a], Shin-ichi Muramatsu [b], Sayaka Asari [b], Imaharu Nakano [b], Koichi Hirata [a]

[a] Department of Neurology, Centre of Sleep Medicine, Dokkyo Medical University School of Medicine, Tochigi, Japan
[b] Division of Neurology, Department of Medicine, Jichi Medical University, Tochigi, Japan

## ARTICLE INFO

## ABSTRACT

Objectives: Transcranial sonography (TCS) has been shown to reveal hyperechogenicity of the substantia nigra (SN) in people with Parkinson's disease and in approximately 10% of healthy subjects. It is hypothesized that SN hyperechogenicity in healthy subjects and patients with idiopathic rapid eye movement (REM) sleep behaviour disorder (iRBD) patients is a marker of vulnerability for Parkinson's disease.
Methods: TCS and positron emission tomography (PET) with 6-[18F] fluoro-meta-tyrosine (FMT), which can assess the level of the presynaptic dopaminergic nerve, were performed in 19 male patients with iRBD, mean age 66.4 (standard deviation [SD] 4.9) years, to assess nigrostriatal function.
Results: Nine patients had pathological SN hyperechogenicity (mean age 66.8 [SD 3.9] years; 0.31 [SD 0.12] $cm^2$) and 10 patients did not have SN hyperechogenicity (mean age 66.0 [SD 5.8] years; 0.11 [SD 0.06] $cm^2$). FMT uptake at the putamen and caudate was significantly lower in iRBD patients with pathological SN hyperechogenicity compared with those without SN hyperechogenicity. However, no correlation was found between SN echogenicity and FMT uptake. This is in conflict with previous findings which showed that subjects with hyperechogenicity had lower FMT uptake in the striatum.
Conclusion: Pathological hyperechogenic alterations in the SN in patients with iRBD may suggest the existence of preclinical SN dysfunction as determined by FMT-PET.

© 2011 Elsevier B.V. All rights reserved.

## 1. Introduction

Rapid eye movement (REM) sleep behaviour disorder (RBD) is a parasomnia characterised by dream-enacting behaviours, unpleasant dreams and lack of muscle atonia during REM sleep. RBD may be idiopathic or related to neurological disease [1]. Patients with idiopathic RBD (iRBD) have been reported to be at increased risk for developing Parkinson's disease (PD) [2]. Transcranial sonography (TCS) has been shown to reveal hyperechogenicity of the substantia nigra (SN) in patients with PD and in approximately 10% of healthy subjects, and has been suggested as a risk marker for PD in non-Parkinsonian subjects [3]. However, Berg et al. reported that SN hyperechogenicity in the elderly is non-specific and of limited usefulness in predicting an individual's risk for PD [4]. Recently, two case-control studies [5,6] showed that pathological SN hyperechogenicity was significantly more common in patients with iRBD compared to control subjects. iRBD is regarded as one of the non-

motor symptoms of PD, and precedes motor symptoms. Schenck et al. identified the development of Parkinsonism in 11 of 29 men initially diagnosed with iRBD [7]. It is hypothesized that SN hyperechogenicity in healthy subjects and patients with iRBD is a vulnerability marker for PD. Although there is strong evidence that the echo originates from increased local iron content, the exact pathophysiological mechanisms for SN hyperechogenicity are not completely understood.

In order to verify the hypothesis that hyperechogenic alterations in the SN may be suggestive of preclinical nigrostriatal dopaminergic dysfunction for patients with iRBD, this study evaluated the presynaptic dopaminergic function in the striatum using 6-[18F] fluoro-meta-tyrosine (FMT) positron emission tomography (PET).

## 2. Methods

This study was performed in accordance with the Declaration of Helsinki. Procedures were approved by the Ethics Review Committee of Dokkyo Medical University, and informed consent was obtained from each subject. TCS and 6-[18F]FMT PET were performed in 19 males with iRBD confirmed by polysomnography.

The mean age of subjects was 66.4 (standard deviation [SD] 4.9) years, the mean estimated duration of RBD was 3.5 (SD 1.8) years, the mean score on the Mini-Mental State Examination (MMSE) was 28.4 (SD 2.0), and the mean score on the Unified Parkinson's Disease Rating Scale (UPDRS) part III was 0.9 (SD 1) (range 0–3). Subjects were recruited from a sleep disorders clinic at Dokkyo Medical University Hospital between July 2008 and 2010. All had a history of recurrent dream-enacting behaviours, and RBD was diagnosed according to the International Classification of Sleep Disorders, second edition [8].

### 2.1. 6-[$^{18}$F] Fluoro-meta-tyrosine positron emission tomography

The PET radiotracer FMT is a substrate of the dopamine-synthe-sizing enzyme. Most FMT signals result from tracer that has been metabolized by aromatic amino acid decarboxylase (AADC) and monoamine oxidase-A, and is trapped in axon terminals as 6-flu-oro-m-hydrophenylacetic acid without being released or further processed. FMT signals represent the extent of AADC activity more fully [9,10].

For 6-[$^{18}$F]FMT PET, the subject was placed on the scanner bed in a GEMINI-TF64 (Philips, Amsterdam, The Netherlands) in the su-pine position. 6-[$^{18}$F]FMT (weight × 0.12 mCi) was injected intra-venously using a syringe pump. Carbidopa pretreatment was used (weight × 2.5 mg). A 10-min static scan was obtained 80 min following injection of 6-[$^{18}$F]FMT. 6-[$^{18}$F]FMT PET and mag-netic resonance imaging (MRI) scans were fused using a Putamen Analyzer (WebNet Technology, Nasushiobara, Japan). Regions of interest were placed manually at the perimeters of the right/left putamen, caudate and cerebellum in MRI scans of the same sub-jects. Right/left putamen:cerebellum (putamen) or caudate:cere-bellum (caudate) ratios of 6-[$^{18}$F]FMT-derived radioactivity were estimated. The sizes of the regions of interest were not fixed. Tissue concentrations of 6-[$^{18}$F]FMT-derived radioactivity (in mCi/cc) were adjusted for the dose per unit of body mass and expressed in units of mCi-kg/cc-mCi (Fig. 1A and B).

### 2.2. Transcranial sonography

TCS was performed using a conventional transcranial Doppler sonograph equipped with a 2.5-MHz phased-array transducer as described previously [5]. Hyperechogenic areas on both sides were analysed separately. To compare areas of echogenicity and the fre-quency of hyperechogenicity, the side of the midbrain (right or left) with the greater area of SN echogenicity in each subject was used for these statistical comparisons. Planimetric quantification of the areas of increased echogenicity was done on both sides of the SN independently (Fig. 1C and D). In accordance with previously re-ported cut-off values, areas of echogenicity <0.20 cm$^2$ were classi-fied as normal, and areas of echogenicity ⩾0.20 cm$^2$ were classified as pathological [3].

The mean interval between performance of TCS and FMT-PET was 126.6 (SD 174.8) days. TCS is performed routinely to assess preclinical condition at the study institute. Berg et al. reported that the echogenic area of the SN did not change in the course of PD during a 5-year follow-up study [11]. Therefore, the interval be-tween the performance of TCS and FMT-PET cannot be considered to influence the results.

Clinical examinations, including the MMSE and UPDRS, FMT-PET and TCS were performed independently by physicians who were blinded to the results of other examinations.

### 2.3. Statistical analysis

Values are expressed as mean (SD). *p*-values were determined using the Mann–Whitney *U*-test. A *p*-value <0.05 was taken to

indicate statistical significance. A statistical comparison of factors such as age of patients, MMSE score, UPDRS part III score and 6-[$^{18}$F]FMT uptake was performed between the groups of patients with iRBD based on the presence or absence of pathological SN hyperechogenicity. The Spearman's correlation coefficient was used for analysis of the correlation between the echogenic area of the SN and the degree of 6-[$^{18}$F]FMT uptake.

## 3. Results

Demographic and clinical data on patients with iRBD are sum-marized in Table 1. Nine of the patients with iRBD had pathological SN hyperechogenicity (mean 0.31 [SD 0.12] cm$^2$) and 10 did not have SN hyperechogenicity (mean 0.11 [SD 0.06] cm$^2$). Therefore, the 19 patients were divided into two groups: those with and those without SN hyperechogenicity. Age distributions, MMSE scores, and UPDRS part III scores did not differ significantly between the groups. Evaluation of motor activity using the UPDRS part III score ranged from zero to three points, which did not fulfill the diagnos-tic criteria for probable PD. Compared with the patients without SN hyperechogenicity, the patients with SN hyperechogenicity had significantly lower uptake of 6-[$^{18}$F]FMT in the putamen (mean 4.40 [SD 0.83] and 3.22 [SD 0.98], respectively; *p* = 0.027) and the caudate (mean 3.69 [SD 0.42] and 2.86 [SD 0.82], respectively; *p* = 0.014) (Table 1). However, the echogenic area of the SN did not correlate with the degree of 6-[$^{18}$F]FMT uptake in the putamen (*r* = −0.4465, *p* = 0.0553) or the caudate (*r* = −0.4007, *p* = 0.0891). In addition, the UPDRS part III scores did not correlate with the de-gree of 6-[$^{18}$F]FMT uptake in the putamen (*r* = −0.240, *p* = 0.323), the caudate (*r* = −0.040, *p* = 0.871), or the echogenic area of the SN (*r* = −0.216, *p* = 0.375).

## 4. Discussion

Unger et al. [12] identified a significant association between midbrain hyperechogenicity and iRBD, and reported that two out of five iRBD patients with SN hyperechogenicity had unremarkable findings by presynaptic dopamine transporter imaging with fluoro-propyl-carbomethoxy-iodophenyl-tropane (FP-CIT) single-photon emission computed tomography (SPECT). Iranzo et al. [13] recently reported that $^{123}$I-FP-CIT striatal binding did not correlate with the extent of SN echogenicity in patients with iRBD. In the present study, FMT uptake in the putamen and caudate was significantly lower in iRBD patients with pathological SN hyperechogenicity than in those without SN hyperechogenicity. In contrast to the present results, Iranzo et al. [13] found that patients with SN hyperechogenicity did not have lower tracer uptake compared with patients without SN hyperechogenicity and they did not find a correlation between SN size and tracer uptake.

Booij et al. [14] reported that motor signs of PD started when the decrease in the percentage of $^{123}$I-FP-CIT binding ratios in the putamen was 46–64% using age-corrected data. Spiegel et al. [15] and Doepp et al. [16] reported a lack of correlation between SN echogenicity and striatal FP-CIT uptake in patients with PD. Spiegel et al. [15] hypothesized that the pathogenic substrate of SN hyper-echogenicity is different from that associated with degeneration of dopaminergic SN projection neurons. Berg et al. [11] failed to find evidence of an increase in the size of the echogenic SN area in a 5-year longitudinal study on PD patients with substantial progres-sion of motor symptoms.

On the other hand, Weise et al. [17] reported a significant correlation between the extension of the echogenic SN area and stri-atal β-CIT binding. They discussed the possibility that the extension of SN echogenicity may be a consequence of degeneration of dopaminergic neurons in the SN, rather than an independent and
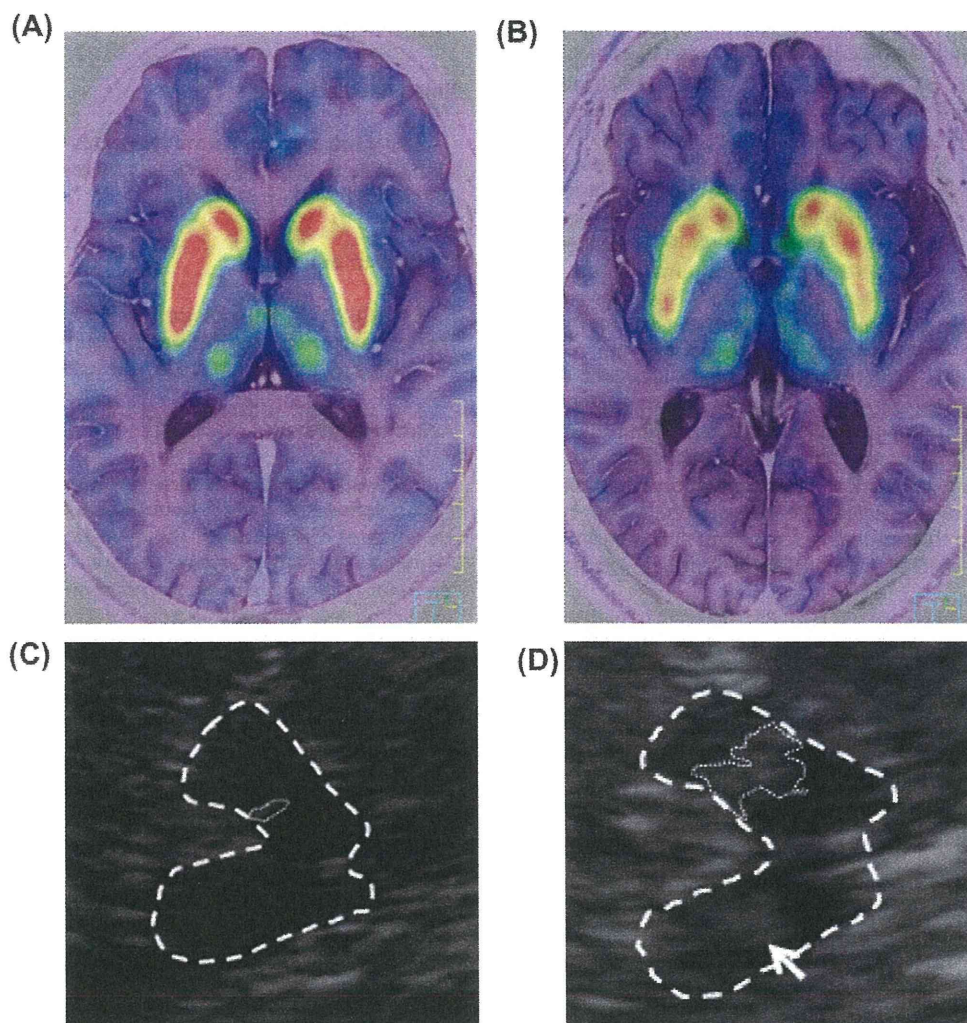
**Fig. 1.** (A) 6-[$^{18}$F] Fluoro-meta-tyrosine positron emission tomography (6-[$^{18}$F]FMT PET) on magnetic resonance imaging (MRI). This demonstrates preserved dopamine terminals in the caudate and putamen in a healthy subject. (B) 6-[$^{18}$F]FMT PET on MRI. This demonstrates patchy decreased dopamine terminals in the caudate and putamen in a patient with idiopathic rapid eye movement sleep behaviour disorder (iRBD). (C) Transcranial sonography (TCS) of bilateral substantia nigra (SN) hyperechogenicity in a healthy subject. The area of hyperechogenic SN signal within the hypo-echogenic crus cerebri is encircled on the ipsilateral side for planimetric measurement (0.10 cm$^2$). (D) TCS of bilateral SN hyperechogenicity in a patient with iRBD. The area of the hyperechogenic SN signal within the hypo-echogenic crus cerebri is encircled on the ipsilateral side for planimetric measurement (0.44 cm$^2$).

**Table 1**
Area of hyperechogenic substantia nigra (SN) signals in two groups of patients with idiopathic rapid eye movement sleep behaviour disorder ($n = 19$).

| | SN hyperechogenicity[*] | | $p$-Value |
|---|---|---|---|
| | Normal (<0.20 cm$^2$) ($n = 10$) | Pathological ($\geqslant 0.20$ cm$^2$) ($n = 9$) | |
| Age (years), mean (SD) | 66.0 (5.8) | 66.8 (3.9) | 0.623 |
| Range, years | 58–77 | 62–72 | N/A |
| Sex, male/female | 10/0 | 9/0 | N/A |
| Estimated duration of RBD (years), mean (SD) | 3.9 (1.7) | 4.3 (2.1) | 0.389 |
| MMSE score, mean (SD) | 28.4 (2.1) | 28.4 (1.9) | 0.864 |
| UPDRS part III score, mean (SD) | 0.9 (1.1) | 1.0 (1.0) | 0.729 |
| *Uptake of 6-[$^{18}$F] FMT, mean (SD)* | | | |
| Putamen | 4.40 (0.83) | 3.22 (0.98) | 0.027 |
| Caudate | 3.69 (0.42) | 2.86 (0.82) | 0.014 |
| Putamen/caudate ratio | 1.19 (0.19) | 1.12 (0.10) | 0.514 |

RBD, rapid eye movement sleep behaviour disorder; MMSE, Mini-Mental State Examination; UPDRS, Unified Parkinson's Disease Rating Scale; FMT, fluoro-meta-tyrosine; SD, standard deviation; N/A, not applicable.
Transcranial sonography (TCS) was considered pathological when SN echogenicity was $\geqslant 0.20$ cm$^2$.
$p$-Value was determined by Mann–Whitney $U$-test.
[*] Side of the midbrain (right or left) with the greater area of SN echogenicity.

mechanistically unrelated phenomenon. SN echogenicity is sensitive to degeneration of dopaminergic neurons. A report by Behnke et al. [18] showed that $^{18}$fluoro-DOPA uptake was lowest in patients with PD, followed by individuals with SN hyperechogenicity, and finally healthy controls without SN hyperechogenicity. The difference was significant between the three groups. Walter et al. [19] reported that brain parenchyma sonography demonstrated SN hyperechogenicity in concordance with abnormal nigrostriatal $^{18}$F-DOPA PET in all symptomatic and three asymptomatic *Parkin* mutation carriers. Thus, they suggested SN hyperechogenicity as an early marker for detection of preclinical Parkinsonism. DelleDonne et al. [20] showed that incidental Lewy body disease (ILBD) has nigrostriatal pathological features that are intermediate between those in pathologically normal persons and patients with PD. Among the participants with ILBD, decreased striatal dopaminergic immunoreactivity was documented for both tyrosine hydroxylase and vesicular monoamine transporter 2 in comparison with the pathologically normal subjects; the reductions were even greater in patients with PD. Also, SN neuronal loss correlated with both striatal vesicular monoamine transporter 2 and tyrosine hydroxylase. Thus, ILBD probably represents presymptomatic PD rather than non-specific, age-related α-synuclein pathological changes.

The current study compared FMT-PET findings in patients with iRBD with and without SN hyperechogenicity. Pathological SN hyperechogenicity in iRBD may be suggestive of nigrostriatal dopaminergic dysfunction, as determined by FMT-PET. However, there was no significant correlation between the area of SN hyperechogenicity and the degree of 6-[$^{18}$F]FMT uptake. It may be that these two parameters have different characteristics. In other words, the area of SN echogenicity is thought to be a stable marker, whereas the uptake of dopaminergic tracer changes progressively with time.

Iranzo et al. found that 19% of 43 patients developed a neurodegenerative syndrome such as PD, dementia with Lewy bodies (DLB), or multiple system atrophy (MSA) 2.5 years after TCS and $^{123}$I-FP-CIT SPECT. They postulated that the combined use of $^{123}$I-FP-CIT SPECT and TCS is a potential strategy for early identification of patients with iRBD who are at risk for development of a synucleinopathy [13]. They also reported that one case of iRBD who developed MSA had decreased striatal $^{123}$I-FP-CIT uptake and normal echogenic SN, and this discrepancy might be explained by the fact that SN hyperechogenicity is less common in MSA than in PD or DLB [13]. Even when SN echogenicity is normal in iRBD, the risk for developing MSA remains. Therefore, patients with iRBD who are at risk for developing not only PD or DLB, but also MSA need to be followed-up.

This study had several limitations. One weak point was that the mean interval between TCS and FMT-PET was approximately four months. Berg et al. reported that the area of SN echogenicity did not change with time in PD [11], but this has not been investigated in patients with iRBD. Due to the lack of a control group in this study, it was not possible to assess if those patients with abnormal PET results had a greater or different echogenic size than those with normal PET results. Satisfactory results of TCS are difficult to obtain in females [5], and all subjects in the study were male. In the future, in order to clarify whether there is a gender difference in the relationship between SN hyperechogenicity and FMT-PET findings, it may be helpful to determine the background of the gender differences in the onset of PD.

Hyperechogenic alterations in the SN may suggest the existence of preclinical SN dysfunction and of an underlying neurodegenerative disorder such as PD or DLB associated with nigrostriatal dysfunction in patients with iRBD. In terms of clinical interest and use of the study findings, there is a need for close clinical follow-up to detect the early signs of a disease characterised by Parkinson-ism, and also to test neuroprotective therapies in the near future in such patients.

## Conflict of interest

The ICMJE Uniform Disclosure Form for Potential Conflicts of Interest associated with this article can be viewed by clicking on the following link: doi:10.1016/j.sleep.2011.03.024.

## References

[1] Boeve BF. REM sleep behavior disorder: updated review of the core features, the REM sleep behavior disorder-neurodegenerative disease association, evolving concepts, controversies, and future directions. Ann NY Acad Sci 2009;1184:15–54.
[2] Postuma RB, Lang AE, Massicotte-Marquez J, Montplaisir J. Potential early markers of Parkinson's disease in idiopathic REM sleep behavior disorder. Neurology 2006;66:845–51.
[3] Berg D. Transcranial ultrasound as a risk marker for Parkinson's disease. Mov Disord 2009;24:S677–83.
[4] Berg D, Seppi K, Liepelt I, et al. Enlarged hyperechogenic substantia nigra is related to motor performance and olfaction in the elderly. Mov Disord 2010;25:1464–9.
[5] Iwanami M, Miyamoto T, Miyamoto M, Hirata K, Takada E. Relevance of substantia nigra hyperechogenicity and reduced odor identification in idiopathic REM sleep behavior disorder. Sleep Med 2010;11:361–5.
[6] Stockner H, Iranzo A, Seppi K, et al. Midbrain hyperechogenicity in idiopathic REM sleep behavior disorder. Mov Disord 2009;24:1906–9.
[7] Schenck CH, Bundlie SR, Mahowald MW. Delayed emergence of a parkinsonian disorder in 38% of 29 older men initially diagnosed with idiopathic rapid eye movement sleep behavior disorder. Neurology 1996;46:388–93.
[8] American Academy of Sleep Medicine. International Classification OF Sleep Disorders. 2nd ed. Diagnosis and coding manual. Westcheste, IL: American Academy of Sleep Medicine; 2005. p. 148–52.
[9] Braskie MN, Wilcox CE, Landau SM, et al. Relationship of striatal dopamine synthesis capacity to age and cognition. J Neurosci 2008;28:14320–8.
[10] Muramatsu S, Fujimoto K, Kato S, et al. A phase I study of aromatic L-amino acid decarboxylase gene therapy for Parkinson's disease. Mol Ther 2010;18:1731–5.
[11] Berg D, Merz B, Reiners K, Naumann M, Becker G. Five-year follow-up study of hyperechogenicity of the substantia nigra in Parkinson's disease. Mov Disord 2005;20:383–5.
[12] Unger MM, Möller JC, Stiasny-Kolster K, et al. Assessment of idiopathic rapid-eye-movement sleep behavior disorder by transcranial sonography, olfactory function test, and FP-CIT-SPECT. Mov Disord 2008;23:596–9.
[13] Iranzo A, Lomena F, Stockner H, et al. Decreased striatal dopamine transporter uptake and substantia nigra hyperechogenicity as risk markers of synucleinopathy in patients with idiopathic rapid-eye-movement sleep behaviour disorder: a prospective study. Lancet Neurol 2010;9:1070–7.
[14] Booij J, Bergmans P, Winogrodzka A, Speelman JD, Wolters EC. Imaging of dopamine transporters with [$^{123}$I]FP-CIT SPECT does not suggest a significant effect of age on the symptomatic threshold of disease in Parkinson's disease. Synapse 2001;39:101–8.
[15] Spiegel J, Hellwig D, Mollers M, et al. Transcranial sonography and [$^{123}$I]FP-CIT SPECT disclose complementary aspects of Parkinson's disease. Brain 2006;129:118–9.
[16] Doepp F, Plotkin M, Siegel L, et al. Brain parenchyma sonography and $^{123}$I-FP-CIT SPECT in Parkinson's disease and essential tremor. Mov Disord 2008;23:405–10.

[17] Weise D, Lorenz R, Schliesser M, Schirbel A, Reiners K, Classen J. Substantia nigra echogenicity: a structural correlate of functional impairment of the dopaminergic striatal projection in Parkinson's disease. Mov Disord 2009;24:1669–75.

[18] Behnke S, Schroeder U, Dillmann U, et al. Hyperechogenicity of the substantia nigra in healthy controls is related to MRI changes and to neuronal loss as determined by F-Dopa PET. NeuroImage 2009;47:1237–43.

[19] Walter U, Klein C, Hilker R, Benecke R, Pramstaller PP, Dressler D. Brain parenchyma sonography detects preclinical parkinsonism. Mov Disord 2004;19:1445–9.

[20] DelleDonne A, Klos KJ, Fujishiro H, et al. Incidental Lewy body disease and preclinical Parkinson disease. Arch Neurol 2008;65:1074–8.

# Compensatory Regulation of Dopamine after Ablation of the Tyrosine Hydroxylase Gene in the Nigrostriatal Projection*[S]

Hirofumi Tokuoka[‡1], Shin-ichi Muramatsu[§], Chiho Sumi-Ichinose[¶], Hiroaki Sakane[‡], Masayo Kojima[‡], Yoshinori Aso[‡], Takahide Nomura[¶], Daniel Metzger[∥**‡‡], and Hiroshi Ichinose[‡2]

From the [‡]Department of Life Science, Graduate School of Bioscience and Biotechnology, Tokyo Institute of Technology, 4259 B-7, Nagatsuta, Midori-ku, Yokohama, 226-8501 Japan, the [§]Division of Neurology, Department of Medicine, Jichi Medical University, Tochigi 329-0498, Japan, the [¶]Department of Pharmacology, School of Medicine, Fujita Health University, Toyoake, Aichi 470-1192, Japan, the [∥]Institut de Génétique et de Biologie Moléculaire et Cellulaire, Illkirch F-67400, France, **CNRS, Illkirch, France , and the [‡‡]Université Louis Pasteur, Strasbourg F-67000, France

**Background:** The tyrosine hydroxylase (TH) gene, essential for dopamine synthesis, is partially ablated in adult nigrostriatal projection.
**Results:** TH reduction in axon terminals is slower than in soma, and dopamine is better maintained than TH.
**Conclusion:** Striatal dopamine is compensatorily regulated by axonal TH level and L-DOPA synthesis activity per TH level.
**Significance:** This regulation has potential relevance to pathogenesis of Parkinson disease and other dopamine-related psychiatric disorders.

The tyrosine hydroxylase (TH; EC 1.14.16.2) is a rate-limiting enzyme in the dopamine synthesis and important for the central dopaminergic system, which controls voluntary movements and reward-dependent behaviors. Here, to further explore the regulatory mechanism of dopamine levels by TH in adult mouse brains, we employed a genetic method to inactivate the *Th* gene in the nigrostriatal projection using the Cre-*loxP* system. Stereotaxic injection of adeno-associated virus expressing Cre recombinase (AAV-Cre) into the substantia nigra pars compacta (SNc), where dopaminergic cell bodies locate, specifically inactivated the *Th* gene. Whereas the number of TH-expressing cells decreased to less than 40% in the SNc 2 weeks after the AAV-Cre injection, the striatal TH protein level decreased to 75%, 50%, and 39% at 2, 4, and 8 weeks, respectively, after the injection. Thus, unexpectedly, the reduction of TH protein in the striatum, where SNc dopaminergic axons innervate densely, was slower than in the SNc. Moreover, despite the essential requirement of TH for dopamine synthesis, the striatal dopamine contents were only moderately decreased, to 70% even 8 weeks after AAV-Cre injection. Concurrently, *in vivo* synthesis activity of L-dihydroxyphenylalanine, the dopamine precursor, per TH protein level was augmented, suggesting up-regulation of dopamine synthesis activity in the intact nigrostriatal axons. Collectively, our conditional *Th* gene targeting method demonstrates two regulatory mechanisms of TH in axon terminals for dopamine homeostasis *in vivo*: local regulation of TH protein amount independent of soma and trans-axonal regulation of apparent L-dihydroxyphenylalanine synthesis activity per TH protein.

---

The dopaminergic system is important for many brain functions, including voluntary movements (1) and reward-related behaviors (2). The dysfunction of dopaminergic transmission is involved in many neurological and psychiatric disorders, such as Parkinson disease (3), addiction (4), attention deficit hyperactive disorders (5), and schizophrenia (6). Although chronic alterations in the dopaminergic system may be relevant to these disorders, it is still unclear how the dopaminergic system is regulated over days to months. In Parkinson disease, motor symptoms exhibit only after a large loss of striatal dopamine (7), suggesting compensation for the loss of dopamine. Although studies on Parkinson disease have suggested multiple forms of compensatory mechanisms, including enhanced dopamine release and turnover (8, 9, 10, 11), it is not fully understood what cellular and molecular mechanisms underlie the long term regulation of striatal dopamine levels under non-degenerative conditions.

Chronic intervention in the dopamine system has been performed for many years by pharmacological methods although they exhibit limitations related to dose dependence, drug metabolism, and circuit specificity. Gene-targeting methods, including germ line knock-out mice (12–14) and dopamine-deficient mice (15–17), have been generated, but because dopaminergic transmissions are blocked from the early stage of brain development, these methods may induce developmental effects. To explore the regulatory mechanisms of the nigrostriatal dopaminergic system in the adult brain, we generated mice in which dopamine synthesis can be selectively abrogated in a spatio-temporally controlled manner. The nigrostriatal projection is the largest dopaminergic projection in the brain, and the dense dopaminergic axon terminals in the striatum are readily

investigated in isolation from their cell bodies and dendrites. Because tyrosine hydroxylase (TH)[3] is the rate-limiting enzyme in dopamine biosynthesis (18), we generated transgenic mice that contain two *loxP* sites flanking the major coding exons of the *TH* gene (floxed *Th* mice).

A microinjection of adeno-associated viral (AAV) vector expressing Cre recombinase (AAV-Cre) (19, 20) into the substantia nigra pars compacta (SNc) of the floxed *Th* mice disrupted the expression of the *Th* gene in a subset of neurons in the SNc of the adult mice. Our biochemical and histochemical analyses suggest two regulatory mechanisms of axonal TH for dopamine homeostasis in the nigrostriatal projection. First, the TH protein level in axon terminals is regulated differently from that in soma. Second, *in vivo* apparent L-DOPA synthesis activity per TH protein level in a given axon is influenced by dopamine synthesis in the neighboring axons, which we propose as trans-axonal regulation of dopamine levels.

## EXPERIMENTAL PROCEDURES

*Production of Th Floxed Mice, Genotyping*—To construct the targeting vector for generating a floxed *Th* allele, a 9.5-kb XhoI-EcoRI genomic DNA segment containing genomic *Th* DNA was isolated from a λ phage 129SV mouse genomic library. The EcoRI site located at the 3′-end was replaced by MluI, a HindIII restriction site was engineered by site-directed mutagenesis between exons 5 and 6, and the SpeI site located between exons 9 and 10 was converted into a NotI site. A *loxP* site and an EcoRV restriction site were inserted into a HindIII site, and a neomycin-resistant cassette, flanked by *loxP* sites, was inserted into a NotI site. The three *loxP* sites in the final targeting vector were in the same orientation (3′ to 5′) (Fig. 1A).

Mouse embryonic stem cells were electroporated with the targeting vector, and the homologously recombined clones were screened by PCR and Southern blot analysis. Embryonic stem clones with three *loxP* sites were selected, and a plasmid expressing Cre DNA recombinase was transiently transfected into the cells. Embryonic stem cells with two *loxP* sites without a neomycin cassette were selected by PCR and used for production of chimeric mice.

The genotypes of mice were identified on mouse ear biopsies by PCR (30 cycles at 94 °C for 30 s, 65 °C for 3 min, and a final extension at 72 °C for 5 min) with primers TH9F (5′-CATTT-GCCCAGTTCTCCCAG-3′) and TH10R (5′-AGAGATG-CAAGTCCAATGTC-3′). The sizes of the PCR products amplified from the wild-type *Th* allele and from the floxed *Th* allele are 431 and 513 bp, respectively.

For the detection of recombined *Th* alleles, genomic DNA was extracted from the substantia nigra regions of brain slices fixed by paraformaldehyde. The recombined *Th* alleles were detected by PCR (30 cycles at 94 °C for 30 s, 66 °C for 30 s, 72 °C

for 1 min 15 s, and a final extension at 72 °C for 5 min) with primers TH5F (5′-AGGCGTATCGCCAGCGCC-3′) and TH10Rb (5′-CCCCAGAGATGCAAGTCCAATGTC-3′). The sizes of the PCR products amplified from the wild-type *Th* allele, floxed *Th* allele, and deleted *Th* allele are 1722, 1886, and 430 bp, respectively.

*AAV Vector Construction*—We generated two types of AAV-Cre vectors basically as described previously (19). One was the AAV-Cre vector, which contained an expression cassette with a human cytomegalovirus immediate early promoter (CMV promoter), followed by the first intron of human growth hormone, Cre recombinase cDNA, and simian virus 40 polyadenylation signal sequence (SV40 poly(A)), between the inverted terminal repeats of the AAV-2 genome. The other was the AAV-GFP/Cre vector, which contained an expression cassette with a synapsin I promoter (21), followed by AcGFP1 (Clontech), the internal ribosomal entry site, Cre recombinase cDNA, and simian virus 40 polyadenylation signal sequence (SV40 poly(A)), between the inverted terminal repeats of the AAV-1 genome. The two helper plasmids, pHLP19 and pladeno1 (Avigen, Alameda, CA), harbored the AAV *rep* and *cap* genes as well as the E2A, E4, and VA RNA genes of the adenovirus genome, respectively. HEK293 cells were co-transfected with the vector plasmid, pHLP19, and pladeno1 by the calcium phosphate precipitation method. The AAV vectors were then harvested and purified by two rounds of continuous iodoxale ultracentrifugations. Vector titers were determined by quantitative DNA dot-blot hybridization or by quantitative PCR of DNase I-treated vector stocks. We routinely obtained $10^{12}$ to $10^{13}$ vector genome copies/ml.

*Animals and Stereotaxic Microinjections*—Mice were acclimated to and maintained at 25 °C under a 12-h light/dark cycle (light on 08:00–20:00). All animal experiments were performed in accordance with the general guidelines of the Tokyo Institute of Technology. Unilateral injections into the SNc were performed on 12–16-week-old mice that were anesthetized with Nembutal (intraperitoneally) and mounted into a stereotaxic apparatus. The coordinates were 3.0 mm posterior from bregma, 1.0 mm lateral to midline, and 4.0 mm ventral from the dural surface. 1 μl of AAV-Cre or AAV-GFP/Cre (about $10^9$ particles) was injected through an injection cannula (28-gauge) with a Hamilton microsyringe driven by a microdialysis pump at a rate of 0.2 μl/min. After microinjection, the injection cannula was left for 2 min before its withdrawal to reduce the efflux of injected liquid along the injection tract. When a cannula was blocked or leaked, the mouse was excluded from the following experiments. The mice were sacrificed at 1, 2, 4, 8, or 16 weeks after microinjection for analyses. We used the uninjected side of a brain as a control side to compare with. $Th^{+/+}$ mice were used as control animals.

*Immunohistochemistry*—Striatal slices were prepared by transcardial perfusion with saline, followed by 4% paraformaldehyde, 60 mM phosphate buffer, and postfixation overnight. All solutions were used at 4 °C. In some experiments, striatal tissues were dissected and homogenized for Western blot and monoamine assay (see below), and the rest of the brain, including the midbrain with the SNc region, was fixed by immersing in 4% paraformaldehyde, PBS overnight. The fixed brain pieces

---

[3] The abbreviations used are: TH, tyrosine hydroxylase; AADC, aromatic L-amino acid decarboxylase; AAV, adeno-associated virus; AAV-Cre, adeno-associated virus expressing Cre recombinase; DA, dopamine; DAT, dopamine transporter; DOPAC, 3,4-dihydroxyphenylacetic acid; HVA, homovanillic acid; L-DOPA, L-dihydroxyphenylalanine; vMAT2, vesicular monoamine transporter 2; SNc, substantia nigra pars compacta; 6-OHDA, 6-hydroxydopamine; GBR12909, 1-[2-[bis-(4-fluorophenyl)methoxy]ethyl]-4-(3-phenylpropyl)piperazine dihydrochloride.

were cryoprotected by 30% sucrose, and the coronal slices of 30-$\mu$m thickness were cut by a cryostat. The free floating serial coronal sections, from the rostral to the caudal edge of SNc or a part of the striatum, were incubated with rabbit anti-TH antibody (1:10,000; Millipore) or rabbit anti-AADC serum (1:20,000) (12), followed by biotinylated goat anti-rabbit IgG antibody (1:250; Vector Laboratories) and avidin-peroxidase complex (Vectastain ABC kit, Vector Laboratories). Immunocomplexes were visualized by a reaction with 3,3′-diaminobenzidine tetrahydrochloride and 0.003% $H_2O_2$. Images were taken using an upright microscope (Eclipse E800, Nikon) equipped with a cooled CCD camera (VB-6010, Keyence).

The numbers of TH-positive neurons in the injected and uninjected side SNc were compared using a stereological cell counting method. SNc was defined according to the brain atlas (22). Briefly, one in every three coronal sections covering the whole SNc was selected (typically 12–14 sections) and stained for TH, and magnified images of SNc were taken using a 20× objective lens (numerical aperture 0.5). For each region of interest, images were taken at multiple different focus planes to visualize all cells in the thickness. The number of all TH-positive cells in SNc in each slice was counted manually with ImageJ (National Institutes of Health). Only cells with an apparently visible nucleus were included. The number of all TH-positive neurons from a set of slices was summed (typically 1600–2000 cells in the uninjected side), and the ratio of the number in the injected side to that in the uninjected side was evaluated.

For fluorescence immunohistochemistry, the following secondary antibodies were used: Alexa546-conjugated anti-mouse IgG (1:2,000; Invitrogen) and Alexa633-conjugated anti-rabbit IgG (1:2,000; Invitrogen). Images were taken using the TCS SPE confocal microscope (Leica) with a 63× oil objective lens and excitation lasers of 532 and 635 nm.

For the detection of dopamine, we fixed mice transcardially with 5% glutaraldehyde, and the brain sections made with vibratome were stained with rabbit anti-TH antibody or rabbit anti-dopamine-glutaraldehyde conjugate (1:500; Millipore). Because glutaraldehyde fixation induces very strong background fluorescence, we performed immunodetection with the avidin-peroxidase complex as described above instead of fluorescence detection.

*Western Blotting*—To dissect striatal tissues for biochemical assays, we first made a coronal section of 2-mm thickness from approximately +1.5 to 0.5 mm to the bregma using a brain matrix (Neuroscience, Inc., Tokyo). Then the left and right dorsal striata were dissected by a surgical blade under a stereo microscope and homogenized using the Pellet Mixer (TreffLab) in 150 $\mu$l of PBS containing 1 mM dithiothreitol, 2 mM EDTA, 2 mM NaF, 1 $\mu$g/ml leupeptin, 1 $\mu$g/ml pepstatin, 1 mM phenylmethylsulfonyl fluoride, and 0.1 mM pargyline, followed by centrifugation at 20,000 × g for 10 min at 4 °C. An aliquot of the supernatant was used for the monoamine assay. In some experiments, ventral midbrain homogenates were prepared similarly, except the positions of coronal sections were approximately −2.5 to −4.5 mm to the bregma. The striatal or ventral midbrain homogenates containing 10 $\mu$g of protein were separated by electrophoresis on a 10% SDS-polyacrylamide gel and transferred to a PVDF membrane. The membranes were

immunodetected using the following primary antibodies: rabbit anti-TH antibody (1:10,000; Millipore), rabbit anti-AADC antibody (1:20,000) (12), or mouse anti-$\beta$-actin antibody (1:10,000; Sigma-Aldrich). Immunoreactive proteins were detected by peroxidase-conjugated secondary antibodies and Immobilon-Western (Millipore). Quantitative analyses were performed with LAS-3000 (Fujifilm).

For better quantification of low level TH proteins by Western blot, we assessed the linearity of the detection using serial dilution of striatal homogenates of the uninjected side (supplemental Fig. 1). Then we employed a range showing a linear relationship between actual loaded proteins (2.5–20 $\mu$g, or a 0.125–1.0 ratio) and measured TH protein levels (0.05–1 ratio). Within this range, we made a standard curve and calibrated the TH protein levels accordingly.

For detection of vesicular monoamine transporter 2 (vMAT2) and dopamine transporter (DAT) proteins, a crude synaptosomal fraction was prepared by homogenizing striatal tissues in 4 mM HEPES buffer containing 0.32 M sucrose, 2 mM NaF, 1 $\mu$g/ml leupeptin, 1 $\mu$g/ml pepstatin, 1 mM phenylmethylsulfonyl fluoride, and 0.1 mM pargyline. The homogenate was centrifuged at 900 × g, the supernatant was further centrifuged at 14,500 × g, and the resulting pellet (P2 fraction) was dissolved in 80 $\mu$l of the same HEPES buffer containing 1% SDS. Protein concentration was determined by the DC protein assay (Bio-Rad). 20 $\mu$g of each protein sample was analyzed by Western blot using the following primary antibodies: rabbit anti-vMAT2 antiserum (1:500; Synaptic Systems), rabbit anti-DAT antibody (1:500; Millipore), rabbit anti-TH antibody (1:10,000; Millipore), or mouse anti-$\beta$-actin antibody (1:10,000; Sigma-Aldrich).

For the detection of phospho-TH proteins, striatal homogenates were prepared by immediate boiling of a whole brain for 5 min after dissection, followed by isolation of striata and homogenization and sonication in 0.1 M Tris-HCl (pH 6.8) buffer containing 1% SDS. Protein concentration was determined by the DC protein assay (Bio-Rad). 60 $\mu$g of each protein sample was analyzed by Western blot using the following primary antibodies: rabbit anti-Ser(P)-40-TH antibody (1:2,000; Millipore), rabbit anti-p31-TH antibody (1:2,000; Millipore), or rabbit anti-TH antibody (1:10,000; Millipore).

*Monoamine Assay*—Aliquots of striatal supernatant were deproteinized by 60 mM perchloric acid with 30 $\mu$M EDTA and 30 $\mu$M pargyline on ice for 30 min and centrifuged at 20,000 × g for 15 min. The monoamine levels in the supernatant were analyzed by high performance liquid chromatography (HPLC) with an SC5-ODS column (EICOM) and a mobile phase buffer containing 84 mM acetic acid-citrate (pH 3.5), 5 $\mu$g/ml EDTA, 190 mg/ml sodium 1-octane sulfonate, and 16% methanol. Monoamines were detected by electrochemical detection (ECD-100, EICOM).

Biopterin contents were measured as described previously (43). Briefly, the deproteinized homogenates were oxidized by 0.1 M HCl containing 0.1% $I_2$ and 0.2% KI for 1 h at room temperature, followed by centrifugation at 20,000 × g for 10 min. The supernatants were neutralized by 0.2% ascorbic acid and then subjected to HPLC analyses with Inertsil ODS-3 column (GL Sciences) and a mobile phase buffer containing 10 mM
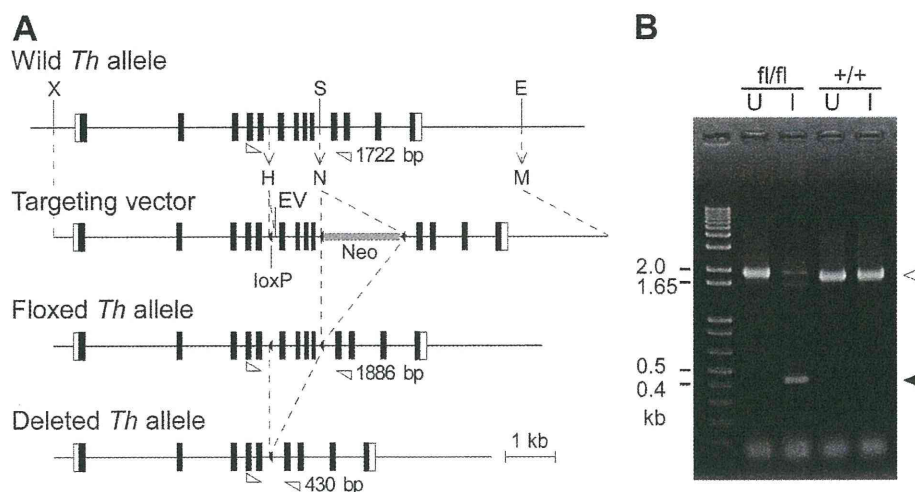
FIGURE 1. **Ablation of the *Th* gene by AAV-Cre injection into the SNc of the floxed *Th* mice.** *A,* schematic representation of the targeting vector for the generation of the floxed *Th* allele. *E,* EcoRI; *H,* HindIII; *M,* MluI; *N,* NotI; *S,* SpeI; *X,* XhoI; *Neo,* neomycin-resistant cassette. *Broken arrows* represent the generation or replacement of a restriction site. Exons are represented by *boxes*. The positions of the primers designed for the detection of genomic DNA recombination by PCR are indicated by *open triangles* with resulting PCR product sizes. *B,* PCR detection of genomic DNA recombination using primers for wild type (*open arrowhead*) or deleted *Th* (*closed arrowhead*) alleles. The template genomic DNA was prepared from the uninjected (*U*) or injected (*I*) side of the of the $Th^{fl/fl}$ or $Th^{+/+}$ mice 2 weeks after the unilateral microinjection of the AAV-Cre into the SNc. Note that the *Th* gene recombination was detected only in the injected side of the SNc of the $Th^{fl/fl}$ mice but not in the uninjected side of the $Th^{fl/fl}$ mice and the $Th^{+/+}$ mice.

NaPO$_4$ (pH 6.9) and a fluorescence detector (excitation 350 nm/emission 440 nm; RF-10A, Shimadzu, Tokyo).

*Estimation of in Vivo L-DOPA Synthesis Activity per TH Protein Level—In vivo* L-DOPA synthesis activity was evaluated by measuring the L-DOPA levels that accumulated in 30 min after the administration of 3-hydroxybenzylhydrazine dihydrochloride (NSD-1015, Sigma-Aldrich), an AADC inhibitor, to mice (100 mg/kg, intraperitoneal). The striatal tissues were homogenized using a pellet mixer (TreffLab) in 150 $\mu$l of PBS containing 1 mM dithiothreitol, 2 mM EDTA, 2 mM NaF, 1 $\mu$g/ml leupeptin, 1 $\mu$g/ml pepstatin, 1 mM phenylmethylsulfonyl fluoride, and 0.1 mM pargyline, followed by centrifugation at 20,000 $\times$ *g* for 10 min at 4 °C. An aliquot of the supernatant was used for assaying protein concentration by Bradford method, and Western blot to assess the TH protein levels. Another aliquot was deproteinized by 60 mM perchloric acid with 30 $\mu$M EDTA and 30 $\mu$M pargyline on ice for 30 min and centrifuged at 20,000 $\times$ *g* for 15 min. The supernatant was neutralized by K$_2$CO$_3$, and L-DOPA was purified by Al$_2$O$_3$ powder. The L-DOPA level was analyzed by HPLC with a NUCLEOSIL 100-7C18 reverse-phase column with a mobile phase buffer containing 0.1 M NaPO$_4$ (pH 3.5), 8 $\mu$M EDTA and electrochemical detection. To evaluate the *in vivo* L-DOPA synthesis activity per TH protein, L-DOPA accumulation was normalized to TH protein levels estimated by Western blot.

*Rotation Test—*Mice were placed in a round bowl (25 cm in diameter) for 20 min for acclimation. The mice were administered with 1-[2-[bis-(4-fluorophenyl)methoxy]ethyl]-4-(3-phenylpropyl)piperazine dihydrochloride (GBR12909; Tocris Bioscience; intraperitoneal, 30 mg/kg) and returned to the same bowl, and the behavior was videorecorded. The rotations were counted by visual observation for a 60-min period immediately after intraperitoneal injection. One rotation was defined by the animal completing a 360° turning without turning back in the opposite direction.

*Statistics—*The Mann-Whitney *U* test, Wilcoxon's signed rank test, or Steel's test was used as required. Spearman's rank correlation was used to evaluate a correlation between two groups. *p* values of <0.05 were considered significant. The data are shown as individual data points and mean values or as mean ± S.E., as indicated. Exponential and liner fittings were performed with Igor Pro 6.2 (WaveMetrics).

## RESULTS

*Production of Floxed Th Mice and Th Gene Ablation by AAV-Cre—*First, we generated the floxed *Th* mice ($Th^{fl/fl}$) in which exons 6–9 of the *Th* gene were flanked by *loxP* sites (Fig. 1*A*). We used AAV-Cre to induce DNA recombination *in vivo* by performing a unilateral stereotaxic microinjection of the virus into the SNc of the adult floxed *Th* mice. Microinjection of AAV-Cre into the SNc induced DNA recombination in 2 weeks when we examined the substantia nigra tissue samples by PCR (Fig. 1*B*). *Th* gene recombination was detected in the injected side SNc of the $Th^{fl/fl}$ mice but not in the uninjected side of the $Th^{fl/fl}$ mice and both sides of the $Th^{+/+}$ mice. Thus, the floxed *Th* mice and AAV-Cre enabled us to induce *Th* gene ablation in the adult mouse midbrain.

*Abrogation of TH Protein Expression in SNc Dopaminergic Neurons—*Using immunohistochemistry, we next examined the effect of the AAV-Cre injection on TH protein expression in the SNc. The TH protein immunoreactivity was absent in the majority of neurons in the SNc 2 weeks after the AAV-Cre injection (Fig. 2*A* and *B*). We found that the number of TH-positive dopaminergic neurons normalized to the uninjected side was reduced by as early as 2 weeks, with the mean ratios of 38, 30, and 40% at 2, 4, and 8 weeks after the AAV-Cre injection, respectively, whereas they were unchanged in the $Th^{+/+}$ mice (97% at 8 weeks; Steel's test, *p* = 0.0239, 0.0166, and 0.0061 for the $Th^{fl/fl}$ mice at 2, 4, and 8 weeks, respectively, compared with the $Th^{+/+}$ at 8 weeks; Fig. 2*C*).
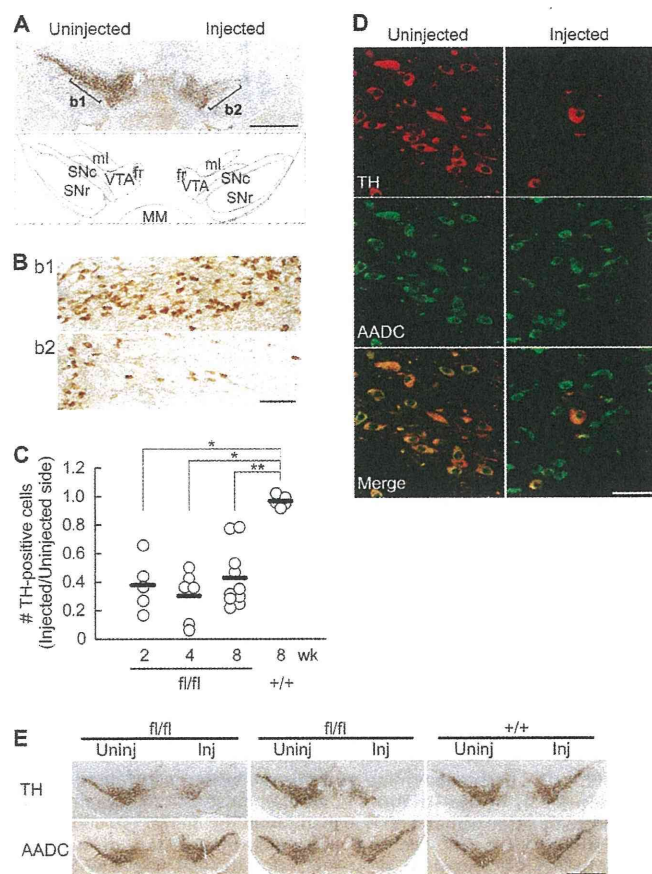
FIGURE 2. **AAV-Cre-induced loss of TH expression in the SNc.** A, a representative image of a midbrain slice immunostained for TH (*top*) and a schematic atlas (*bottom*). Serial coronal sections of the midbrains of the $Th^{fl/fl}$ mice were prepared 8 weeks after the AAV-Cre injection and were immunostained for TH. The SNc in the atlas is indicated by the *hatched area*. *fr*, fasciculus retroflexus; *ml*, medial lemniscus; *MM*, medial mammillary nucleus; *SNr*, substantia nigra pars reticulata; *VTA*, ventral tegmental area. B, magnified views of the uninjected side (*b1*) and injected side (*b2*) SNc as indicated in A. C, summary of the ratio of TH-positive cell numbers in the injected side SNc to the uninjected side. *Open circles* indicate the values from individual animals, and *bars* indicate the means. $n = 5, 6, 11$, and 5 brains for 2, 4, and 8 weeks ($Th^{fl/fl}$ mice) and 8 weeks ($Th^{+/+}$ mice) after injection, respectively. *, $p < 0.05$; **, $p < 0.01$, Steel's test. D, immunofluorescence staining for TH (*red*) and AADC (*green*) of the SNc of the $Th^{fl/fl}$ mice examined 2 weeks after the injection of AAV-GFP/Cre. TH and AADC were visualized with Alexa546 and Alexa633, respectively, distinguishing from GFP signal, and *pseudocolored* confocal images are shown. Note that the number of TH-expressing neurons was clearly reduced in the AAV-GFP/Cre-injected side, whereas the AADC, another dopaminergic neuron marker, remained expressed. E, TH deletion induces no apparent cell death in 16 weeks. Midbrain slices from two $Th^{fl/fl}$ mice and one $Th^{+/+}$ mouse were immunostained for TH and AADC 16 weeks after the AAV-Cre microinjection. Whereas the TH-expressing neurons were reduced in the injected side of the SNc of the $Th^{fl/fl}$ mice, the number of AADC-expressing neurons was apparently unaffected, suggesting that the dopaminergic neurons do not show cell death in the absence of TH in 16 weeks. *Scale bars*, 1 mm (A), 100 μm (B), 50 μm (D), and 1 mm (E).

To confirm a selective loss of TH protein, we also performed double immunofluorescence histochemistry for TH and aromatic AADC, a dopaminergic neuron marker. We used AAV-GFP/Cre for the purpose of labeling infected cells, but GFP expression in these neurons was too weak for detection, so we immunostained TH and AADC with Alexa546 and Alexa633 fluorophores, respectively, distinguishing from GFP signals. We found that the AADC immunoreactivity was preserved in the TH-negative neurons in the SNc 2 weeks after the AAV-

GFP/Cre injection (Fig. 2D), suggesting that the AAV-GFP/Cre injection induced an efficient *Th* gene ablation without inducing cell death or damage. Moreover, AADC expression in the SNc was apparently unaffected in the $Th^{fl/fl}$ mice up to 16 weeks following the AAV-Cre injection, when the majority of the SNc dopaminergic neurons lost TH expression (Fig. 2E). These data suggest that dopamine is not essential for the survival of dopaminergic neurons in adult brains.

*Slower Reduction of TH Proteins in Axon Terminals of Nigrostriatal Projection*—The dopaminergic neurons in the SNc project their axons toward the striatum and form dense synapses (23, 24), where abundant TH proteins were contained. We quantitatively examined the reduction of the TH protein in the striatum by Western blot (Fig. 3A and B). The TH protein level was gradually reduced in the AAV-Cre injected side compared with the uninjected side in $Th^{fl/fl}$ mice, to 75, 50, and 39% at 2, 4, and 8 weeks after the AAV-Cre injection, respectively, whereas the levels were unchanged in the $Th^{+/+}$ mice (104% at 8 weeks; Steel's test, $p = 0.0932, 0.0071$, and $0.0059$ for the $Th^{fl/fl}$ mice at 2, 4, and 8 weeks, respectively, compared with the $Th^{+/+}$ at 8 weeks; Fig. 3B). AADC protein levels did not show significant changes (Steel's test, $p = 0.77, 0.92$, and $0.88$ for the $Th^{fl/fl}$ mice at 2, 4, and 8 weeks, respectively, compared with the $Th^{+/+}$ at 8 weeks; supplemental Fig. 2A).

We noticed that the reduction of TH protein level in the striatum could be slower than the reduction of the number of TH-expressing cells in the SNc because the difference between the two seemed remarkable at 2 weeks. To further investigate the difference, we compared the TH protein reductions in the striatum with that in ventral midbrain tissue, including SNc, using Western blot (Fig. 3C). We found that the TH protein reduction in the striatum showed a delay by about 2 weeks, whereas the decay time constants were similar ($\tau = 2.06$ and $2.04$ weeks for the ventral midbrain and striatum, respectively).

We also used immunofluorescence histochemistry to examine the expression of TH and AADC in the striatum (Fig. 3D). Two weeks after the AAV-Cre injection, the number of TH-expressing axons in the injected side of the striatum of the $Th^{fl/fl}$ mice was only slightly reduced compared with the uninjected side, which was consistent with the Western blot data. However, the number of TH-expressing axons was decreased profoundly 8 weeks after the AAV-Cre injection. The number of AADC-expressing axons was apparently unchanged, suggesting that the axon terminals of the dopaminergic neurons remained mostly intact. These Western blot and immunohistochemical data indicate differential regulation of TH protein levels between axon terminals (striatum) and soma (SNc). Also, the *Th* gene ablation led to an almost complete and selective loss of TH protein in a subset of dopaminergic axons.

*Better Maintenance of Striatal Dopamine Levels than TH Protein Levels*—To investigate if dopamine levels follow the reduction of TH protein levels in the striatum, we assayed striatal monoamine contents using the same striatal extracts used in the Western blot analysis (Fig. 4A). The dopamine contents decreased gradually to around 98, 79, and 69% at 2, 4, and 8 weeks after the AAV-Cre injection, respectively, in the $Th^{fl/fl}$ mice but not in the $Th^{+/+}$ mice (104% at 8 weeks; Steel's test, $p = 0.98, 0.0475$, and $0.0637$ for 2, 4, and 8 weeks in the $Th^{fl/fl}$
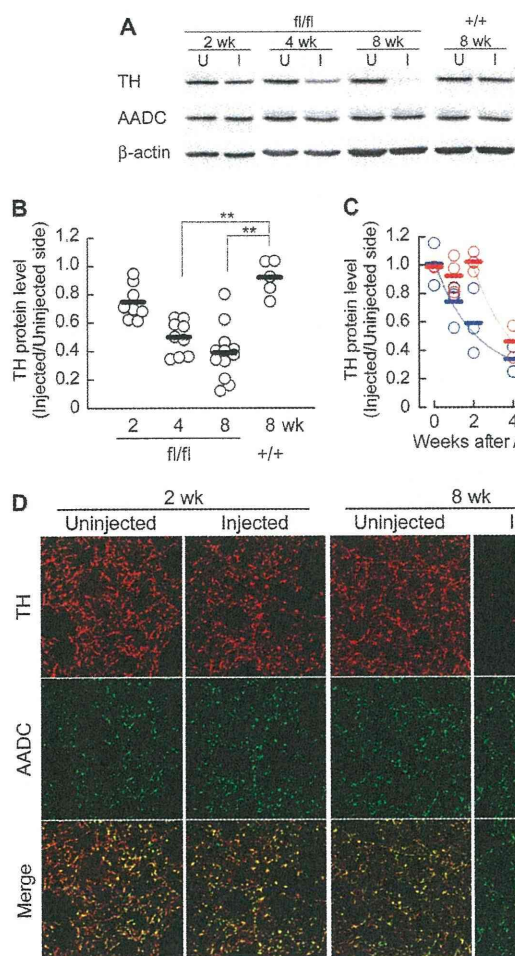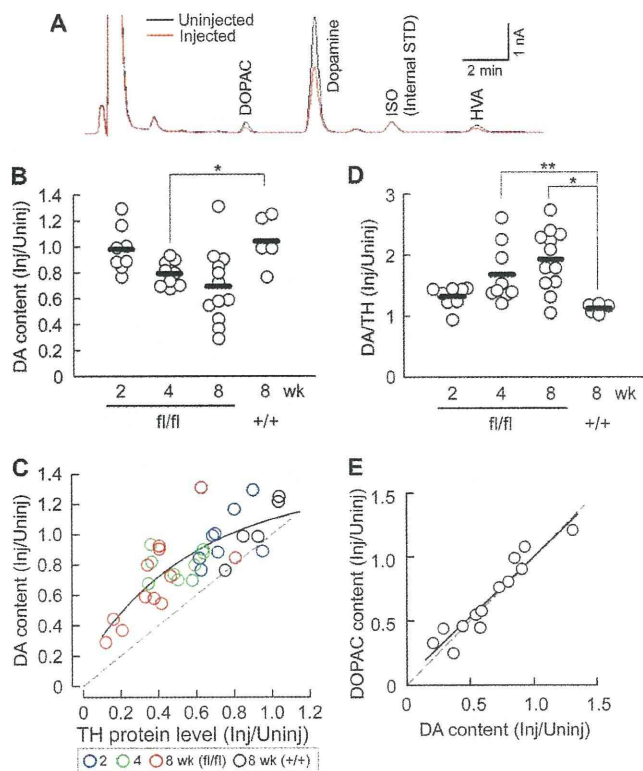
**FIGURE 3. Decrease in striatal TH protein levels after *Th* gene ablation.** *A,* striatal homogenates of each genotype were prepared 2, 4, or 8 weeks after the unilateral AAV-Cre injection into the SNc, and Western blot analysis was performed with antibodies against TH, AADC, and β-actin. *U* and *I,* uninjected and injected sides of the striatum, respectively. *B,* summarized quantitative analyses of Western blots for the striatal TH protein levels. The ratios of the protein level of the injected side to the uninjected side are plotted on the *vertical axis.* The *open circles* indicate the values from individual animals, and the *bars* indicate the means. *n* = 8, 9, 12, and 5 brains for 2, 4, and 8 weeks (*Th*<sup>fl/fl</sup> mice) and 8 weeks (*Th*<sup>+/+</sup> mice) after injection, respectively. *, *p* < 0.05; **, *p* < 0.01, Steel's test. *C,* comparison of TH protein levels in the striatum and ventral midbrain by Western blot. Tissue homogenates were prepared from the injected side and uninjected side of the ventral midbrain (*vMB*) and striatum (*Str*) of *Th*<sup>fl/fl</sup> mice and were subjected to Western blots for TH. *n* = 2, 4, 3, 2, and 3 for 0, 1, 2, 4, and 10 weeks after AAV-Cre injection, respectively. Data were fitted with an *exponential curve.* For the striatum, fitting was performed from 2 weeks because there was no apparent reduction before 2 weeks in this data set. *D,* decrease in the number of TH-expressing axons in the striatum. Striatal slices of the *Th*<sup>fl/fl</sup> mice were prepared 2 and 8 weeks after the injection of AAV-GFP/Cre and were immunohistochemically stained for TH (*red*) and AADC (*green*). TH and AADC were visualized as in Fig. 2*D. Merged images* are shown at the *bottom.* Images from the uninjected and injected side of the striatum are shown as indicated. *Scale bar,* 10 μm.



**FIGURE 4. The tissue dopamine contents are better maintained than TH protein levels in the striatum.** *A,* representative chromatograms of the monoamine assay with the homogenates from the uninjected and injected side striata from a *Th*<sup>fl/fl</sup> mouse 8 weeks after the injection of AAV-Cre. *B,* summarized DA contents in the striatum after the unilateral AAV-Cre injection to the SNc in the *Th*<sup>fl/fl</sup> and *Th*<sup>+/+</sup> mice. The monoamine assays were performed using the same extracts used in Fig. 3. The ratios of the dopamine contents in the injected side to the uninjected side are shown. The *open circles* indicate the values from individual animals, and the *bars* indicate the means. *n* = 8, 9, 12, and 5 brains for 2, 4, and 8 weeks (*Th*<sup>fl/fl</sup> mice) and 8 weeks (*Th*<sup>+/+</sup> mice) after the injection, respectively. *, *p* < 0.05, Steel's test. The mean dopamine contents in the uninjected side striata were 147.2 ± 10.2 and 158.1 ± 6.7 pmol/mg protein for *Th*<sup>fl/fl</sup> and *Th*<sup>+/+</sup> mice, respectively at 8 weeks (Steel's test, *p* = 0.86). *C,* the relationship between dopamine contents and TH protein levels. The *circles* represent data from individual animals and are *color-coded* by weeks after the AAV-Cre injection as indicated. The *dotted line* has a slope of 1. The *solid line* indicates an exponential curve fitting. The *points above* the *dotted line* suggest a higher dopamine level per TH protein level in the injected side compared with the uninjected side. *D,* ratio of the dopamine content to the TH protein level normalized to the uninjected side. *n* = 8, 9, 12, and 5 brains for 2, 4, and 8 weeks (*Th*<sup>fl/fl</sup> mice) and 8 weeks (*Th*<sup>+/+</sup> mice) after the injection, respectively. We excluded one outlier that showed very low TH protein levels and a high DA/TH ratio (29.8) from the 8-week *Th*<sup>fl/fl</sup> group. *, *p* < 0.05; **, *p* < 0.01, Steel's test. *E,* the relationship between DOPAC and dopamine contents in the *Th*<sup>fl/fl</sup> mice 8 weeks after the AAV-Cre injection. The data indicate the ratio of the DOPAC contents in the AAV-Cre-injected side of the striatum normalized to the uninjected side. The *open circles* indicate individual data. The *dotted line* has a slope of 1, and the *solid line* indicates a linear fitting. *n* = 13 mice. Spearman's rank correlation, *p* < 0.0001, ρ = 0.96 for DOPAC *versus* dopamine.
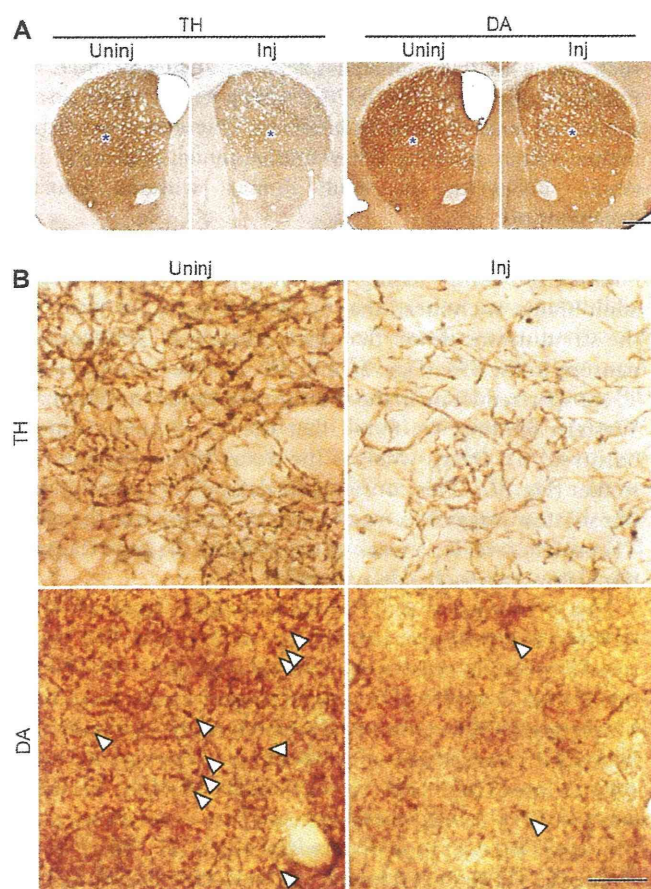
mice, respectively, compared with the *Th*<sup>+/+</sup> mice at 8 weeks; Fig. 4*B*). Notably, these reductions of dopamine contents were not as striking as those of TH protein levels (Fig. 2*C*). To evaluate the relationship between dopamine and TH, we plotted dopamine contents against TH protein levels (Fig. 4*C*). We found that dopamine contents were less affected than the TH protein levels, and the relationship was fitted well with an exponential curve ($\chi^2$ = 0.7391). The dopamine contents did not

show a remarkable reduction until the TH protein levels were decreased by around 50%. Accordingly, the ratios of dopamine contents to TH protein levels were increased, with ratios of 1.32, 1.68, and 1.93 at 2, 4, and 8 weeks after the AAV-Cre injection, respectively, in the *Th*<sup>fl/fl</sup> mice, whereas it remained 1.1 in the *Th*<sup>+/+</sup> mice at 8 weeks (Steel's test, *p* = 0.0665, 0.0071, and 0.0157 for 2, 4, and 8 weeks for the *Th*<sup>fl/fl</sup> mice, respectively, compared with the *Th*<sup>+/+</sup> mice at 8 weeks; Fig. 4*D*).

FIGURE 6. **Enhanced *in vivo* L-DOPA synthesis activity per TH protein level.** L-DOPA synthesis activities per TH protein level were estimated by measuring L-DOPA accumulation after *in vivo* administration of NSD-1015, an AADC inhibitor. Striatal homogenates were prepared 30 min after NSD-1015 administration (100 mg/kg, intraperitoneally). L-DOPA levels were measured by HPLC, and TH protein levels were assayed by Western blot. The mice were examined 8 weeks after the AAV-Cre injection. *A*, summary of L-DOPA accumulation in $Th^{fl/fl}$ and $Th^{+/+}$ mice. Data are shown as L-DOPA level in the injected side normalized by the uninjected side. The *open circles* indicate the values from individual animals, and the *bars* indicate the means. The mean L-DOPA level in the uninjected side of the $Th^{+/+}$ mice was 42.1 ± 7.3 pmol/mg protein. *B*, summary of L-DOPA accumulation normalized to the TH protein levels examined by Western blot, providing apparent L-DOPA synthesis activity per TH protein level. *, $p < 0.05$, Mann-Whitney $U$ test.
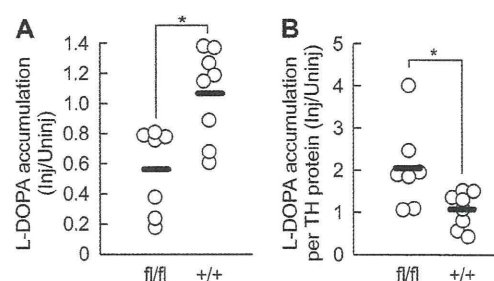


FIGURE 5. **TH and dopamine distribution in the striatum.** *A*, immunohistochemical detection of the striatal TH and DA in the striatum of the $Th^{fl/fl}$ mouse. The mice were fixed with glutaraldehyde 8 weeks after the injection of AAV-GFP/Cre, and the slices cut with a vibratome were stained with antibodies against TH or dopamine. Note that the TH signal in the injected side (*Inj*) was decreased compared with the uninjected side (*Uninj*), whereas the DA signal was less affected. *B*, magnification images of the regions indicated by *asterisks* in *A*, showing TH-expressing axon fibers and dopamine-containing axonal boutons. *Arrowheads* indicate representative puncta of the dopamine signals. *Scale bars*, 0.5 mm (*A*) and 10 μm (*B*).

It is known that unilateral depletion of dopamine in the rodent nigra induces ipsilateral rotation behavior in response to reagents enhancing dopaminergic transmission (25, 26). Consistently, $Th^{fl/fl}$ mice with severe unilateral dopamine depletion showed ipsilateral rotation behavior when administered with GBR12909, a potent DAT inhibitor (supplemental Fig. 2B), demonstrating the validity of our genetic manipulation to disrupt nigrostriatal dopaminergic transmission.

To further examine the tissue level alterations in the dopamine distribution, we used immunohistochemistry to determine the expression pattern for dopamine and TH in the striatum 8 weeks after the AAV-Cre injection. The mice were fixed transcardially with glutaraldehyde, and the striatal slices were stained with an antibody raised against dopamine-glutaraldehyde conjugate. We used immunoenzyme detection instead of immunofluorescence detection, because glutaraldehyde fixation causes a high fluorescence background. At a lower magnification, TH immunoreactivity was clearly reduced in the AAV-Cre-injected side of the $Th^{fl/fl}$ mice, whereas the dopamine immunoreactivity was only moderately reduced (Fig. 5A).

These data are consistent with Western blot and monoamine assay results. Higher magnification views showed a reduction in the number of TH-expressing axon fibers in the AAV-Cre-injected side of the $Th^{fl/fl}$ mice (Fig. 5B) as observed by immunofluorescence staining (Fig. 3D). Moreover, the number of punctate signals of dopamine was also greatly decreased (Fig. 5B), suggesting that dopamine levels in the TH-lost axons were substantially reduced. Collectively, these data indicate a compensatory regulation of dopamine levels for a decrease in the TH protein levels. Because TH expression remained in only a subset of dopaminergic axons, these data raise the possibility that a decrease in dopamine synthesis induces a compensatory upregulation of dopamine synthesis and/or storage in other axons.

*Mechanisms of Dopamine Maintenance against TH Protein Loss*—The homeostatic compensation of dopamine levels may accompany either an increase in the synthesis of dopamine or a decrease in the degradation of dopamine. To examine the degradation rate of dopamine, we measured the contents of 3,4-dihydroxyphenylacetic acid (DOPAC) and homovanillic acid (HVA), the two major metabolites of dopamine. Reductions of DOPAC and HVA contents were well correlated with that of dopamine in the $Th^{fl/fl}$ mice (Fig. 4E). Comparison between injected and uninjected sides showed no difference in the ratio of DOPAC to dopamine (DA) (injected side, 0.12 ± 0.02; uninjected side, 0.15 ± 0.03; Wilcoxon's signed rank test, $p = 0.16$) and in the ratio of HVA to dopamine (injected side, 0.13 ± 0.01; uninjected side, 0.14 ± 0.01; Wilcoxon's signed rank test, $p = 0.43$; supplemental Fig. 3). These data suggest that the degradation rate of dopamine was not significantly changed.

To explore a possible change in the activity of dopamine synthesis pathway, we evaluated *in vivo* L-DOPA synthesis activity by measuring L-DOPA accumulation 30 min after administration of NSD-1015, an AADC inhibitor, 8 weeks after the AAV-Cre injection. We found that the L-DOPA accumulation in the injected side of the striatum was significantly lower in the $Th^{fl/fl}$ mice compared with the $Th^{+/+}$ mice (Mann-Whitney $U$ test, $p = 0.0206$; Fig. 6A). We then estimated the apparent L-DOPA

synthesis activity per TH protein by normalizing the L-DOPA accumulation with TH protein levels estimated by Western blot analysis. We found that the L-DOPA accumulation per TH protein in the injected side striatum was significantly higher in the $Th^{fl/fl}$ mice than in the $Th^{+/+}$ mice (Mann-Whitney $U$ test, $p = 0.0279$; Fig. 6B). Considering that L-DOPA is mostly synthesized by TH (14), and the TH proteins remained to be expressed in only a subset of axons, these data suggest that dopamine synthesis activity in the remaining TH-positive axons was augmented to compensate for dopamine level.

Further, we examined if TH phosphorylation at Ser-31 and Ser-40 (27), the two major phosphorylation sites for TH activation, was elevated. However, we did not find a significant change in the phosphorylation states of these Ser residues by Western blot (supplemental Fig. 4). We also measured the contents of biopterin, an essential cofactor for TH, but the contents were not significantly different between the injected and uninjected side (uninjected side, $6.72 \pm 0.54$ pmol/mg protein; injected side, $6.64 \pm 0.49$ pmol/mg protein; Mann Whitney $U$ test, $p = 0.95$). Thus, the long term up-regulation of L-DOPA synthesis activity may be supported by other molecular mechanisms (*e.g.* a relief of the feedback inhibition of TH by dopamine as a consequence of impaired dopamine synthesis).

In axon terminals, synthesized dopamine is primarily stored in synaptic vesicles, and released dopamine is partly recycled by DAT. When the number of TH-expressing axons was greatly reduced, the manner of dopamine storage could be changed for adaptation. In this context, we examined the level of two major dopamine transporters: vMAT2 and DAT. Western blot analysis showed no significant change in the vMAT2 and DAT protein levels in the injected side striatum compared with the uninjected side in the $Th^{fl/fl}$ mice, despite the great reduction of TH protein levels (supplemental Fig. 5). These data suggest that the numbers of dopaminergic synaptic vesicles and terminals were not grossly altered. Instead, because the majority of dopaminergic axons do not contain normal level of dopamine (Fig. 5B), despite the moderate decrease in tissue dopamine contents (Fig. 4), the vesicular dopamine contents in the TH-expressing axons may be increased, and/or TH-negative axons may uptake and contain low level dopamine.

## DISCUSSION

*Selective Loss of TH Protein in a Subset of Dopaminergic Neurons without Neuronal Degeneration*—We took advantage of the Cre-*loxP* system in mice, which enabled us to selectively ablate the *Th* gene and block dopamine synthesis in adult brains. TH expression in the SNc was lost in a subset of SNc dopaminergic neurons by as early as 2 weeks after the AAV-Cre injection. The TH protein level and the number of TH-expressing axons in the striatum were clearly reduced 8 weeks after the AAV-Cre injection. Severe dopamine deficiency accompanied ipsilateral rotation behavior when stimulated with the DAT inhibitor, GBR12909, confirming the integrity of our genetic method to disrupt nigrostriatal dopaminergic transmission.

In contrast, the AADC protein levels and immunohistochemical signals in the striatum and SNc were unaffected 8 or 16 weeks after the AAV-Cre injection. These data suggest that the SNc dopaminergic neurons and axons were mostly pre-

served for several months without synthesizing dopamine. This is in contrast to neurodegenerative models using neurotoxins, such as 1-methyl-4-phenyl-1,2,3,6-tetrahydropyridine and 6-hydroxydopamine (6-OHDA), which could cause loss of axons and unpredictable side effects. Therefore, our experimental system provides a new animal model of chronic dopamine deficiency in adult brains without neuronal degeneration.

*Differential Regulation of TH Protein Level in the Axon Terminals from Soma*—Using this *Th* gene ablation strategy in adult brains, we noticed that the decline in the TH protein in the striatum was slower than the reduction of TH-expressing neurons in the SNc (Figs. 2C and 3B). By direct comparison of TH protein reduction in the striatum and ventral midbrain with Western blotting, we found that the TH protein reduction occurred in a delay, whereas the decay time constants were similar (Fig. 3C). This considerable delay of TH protein loss in the striatum suggests a mechanism that maintains the axonal TH protein level for a week or two without *Th* gene transcription. How does such a delay occur?

First, the turnover of TH proteins in axon terminals in the striatum may be slower than that in cell bodies in SNc. In cultured chromaffin cells, the steady-state half-life of the TH protein is about 1 day (28), but it could become longer than 10 days by treatment with translational inhibitors (29). Moreover, incubation with transcriptional inhibitors for 3 days caused no significant loss of the TH protein, although 90% of the TH mRNA was lost (29). Axonal translation may be involved for such a prolonged delay of protein degradation (30, 31). Thus, the difference in TH protein turnover in axon terminals and cell bodies located in SNc may be supported by those multiple regulatory mechanisms.

In addition, the delayed reduction of TH proteins may be attributable to slow axonal transport of TH proteins from soma to axons. Although the mechanism underlying axonal TH transport is not fully understood, the projection from SNc to the striatum in mice is about 2–10 mm, depending on axonal branching (22, 23). The axonal transport of TH was reported to be about 2 mm/h in chicken sciatic nerves (32), but it could be different in the brain because the cytosolic proteins are delivered by the slow axonal transport system at 0.1–8 mm/day (33, 34). These reports raise a possibility that it takes a week or more to transport TH proteins from a soma to axon terminals in the mouse nigrostriatal projection.

*Regulation of Dopamine Levels by TH Protein Level and Activity in the Striatum*—By quantitative comparison of dopamine contents with TH protein levels in the same striatal tissues, we found that dopamine contents were not simply determined by the TH protein level only. Notably, even 50% loss of TH protein did not remarkably change the dopamine contents. Eight weeks after the AAV-Cre injection, the TH protein levels were reduced to 39%, on average, whereas the dopamine contents were reduced to 69%. Immunohistochemical data showed a similar trend of difference. This finding is consistent with a previous report that dopamine contents in the brain of the adult $Th^{+/-}$ heterozygous mice are normally maintained despite a significant decrease in TH activity (12). Thus, these data indicate that the dopamine levels were primarily determined by TH

protein level but also influenced by another mechanism in the nigrostriatal projection.

In this study, we showed that (i) the TH protein expression was abrogated in a subset of dopaminergic neurons (AAV-Cre-infected neurons); (ii) the striatal dopamine contents were better maintained than the TH protein levels; and (iii) *in vivo* L-DOPA synthesis activity per TH protein level was enhanced. Because L-DOPA synthesis activity was virtually retained in only the TH-expressing axons, these results suggest that L-DOPA synthesis activity per TH protein in a given axon is partly affected by dopamine synthesis in the neighboring axons. Such trans-axonal regulation of dopamine synthesis activity might be a basis for the homeostasis of dopaminergic transmission in the striatum.

Consistent with our data, in a rat model of preclinical parkinsonism where nigrostriatal dopaminergic neurons were lesioned by 6-OHDA, TH activity was increased relative to dopamine loss (35). In such models generated with 6-OHDA, however, it is difficult to know if the enhanced TH activity observed after 6-OHDA administration is a result of a direct toxic effect of 6-OHDA on the remaining axons, a cell death of neighboring axons, or a decrease in tissue dopamine level. In contrast, our genetic manipulation specifically targets the *Th* gene in AAV-Cre-infected neurons, so our results demonstrate the effect of *Th* gene deletion on TH protein levels, dopamine contents, and L-DOPA synthesis activity more clearly and simply.

It remains to be determined how trans-axonal compensation of dopamine is mediated. For example, TH homospecific activity may be changed for the compensation by phosphorylation. D2 autoreceptors on dopaminergic axon terminals may be involved in controlling the dopamine level (36). However, it is not clear whether D2 autoreceptors modify dopamine synthesis in the long term. For example, chronic administration of haloperidol, a D2 receptor inhibitor, does not increase the basal levels of Ser(P)-31-TH and Ser(P)-40-TH in mice (37). We could not detect significant change in the Ser(P)-31-TH and Ser(P)-40-TH levels.

TH is also controlled by a feedback inhibition loop by dopamine (27). For example, a decrease in extracellular dopamine level by *Th* gene ablation may cause lower dopamine reuptake (38), lower local dopamine concentration in axon terminals, and a relief of TH from the feedback inhibition. Previous reports suggest that the concentration of released dopamine can be on the order of micromolar and is quickly taken up by DAT into dopaminergic axons (38). Because intracellular dopamine concentration is probably <100 nM (39), local intracellular dopamine concentration could be affected by dopamine reuptake. Meanwhile, TH has two dopamine-binding sites: high affinity ($K_d$ < 4 nM) and low affinity ($K_d$ = 90 nM) (40). Therefore, most TH proteins would be the dopamine-bound form for the high affinity site, whereas the low affinity site may be more relevant to feedback inhibition by dopamine (40).

Alternatively, there is a circuit level feedback (8) or neurotrophic factors, such as glial cell-derived neurotrophic factor (41). Further studies will be required to clarify the signaling mechanisms underlying the trans-axonal regulation of dopamine levels.

We found that the ratio of DOPAC and HVA contents to dopamine did not change, whereas, in Parkinson disease patients and model animals, DOPAC/DA and HVA/DA ratios were reported to be increased (7, 10, 42). This difference may exist because in our experimental conditions, most of the dopaminergic axons were preserved after the *Th* gene ablation, and those axons may have participated in the reuptake of extracellular dopamine, resulting in minimal effects on the dopamine degradation rate.

*Adjusting Dopamine Storage for Compensation*—If the number of dopamine-synthesizing axons was decreased by more than half, where and how were dopamine molecules stored for compensation? Because we did not observe any gross changes in the vMAT2 and DAT protein levels, it is unlikely that the numbers of dopaminergic synaptic vesicles and terminals were drastically changed. Otherwise, vesicular dopamine contents may be increased in the remaining TH-expressing axons for the compensation. For example, treatment of cultured dopaminergic neurons with L-DOPA or glial cell-derived neurotrophic factor increased vesicular dopamine levels more than 3-fold (41). Alternatively, it is also possible that the low level dopamine was contained in the TH-negative axons through the reuptake of spilled-over dopamine from neighboring synapses. This mechanism is consistent with the idea that released dopamine is spilled over and taken up by neighboring axons (38). Thus, the compensation of dopamine levels in our experimental system may accompany an increase in vesicular dopamine contents and/or spill-over and reuptake of released dopamine by TH-negative axons.

Taken together, in this study, we develop a conditional gene targeting method to efficiently and selectively inactivate the *Th* gene in the SNc dopaminergic neurons in adult mice without inducing neuronal degeneration. The analysis of these mutant mice revealed that TH protein levels in the axon terminals are regulated differently from the level in the soma, and the tissue dopamine levels are under trans-axonal compensatory regulation, where the reduction of dopamine in some axons induces up-regulation of dopamine synthesis activity in other axons. We believe that the present findings represent at least one of the compensatory mechanisms in Parkinson disease and are related to actions of remedies for psychiatric disorders.

## REFERENCES

1. Graybiel, A. M., Canales, J. J., and Capper-Loup, C. (2000) *Trends Neurosci.* **23,** S71–S77
2. Schultz, W. (2007) *Trends Neurosci.* **30,** 203–210
3. Fahn, S. (2003) *Ann. N.Y. Acad. Sci.* **991,** 1–14
4. Grace, A. A., Floresco, S. B., Goto, Y., and Lodge, D. J. (2007) *Trends*